

**Design of a novel static mixer crystallizer for inland brine management**

By

Joe Costello

B.A. Chemistry, Occidental College, 2019

A Report submitted to the

Faculty of the Graduate School

of the University of Colorado

in partial fulfillment of the requirements for the course of

Master's Thesis

Department of Civil, Environmental, and Architectural Engineering

2023

Committee members

Dr. John Pellegrino

Dr. Julie Korak

Dr. Joe Ryan

## **Abstract**

Costello, Joseph (M.S., Civil , Environmental and Architectural Engineering)

Design of a novel static mixer crystallizer for inland brine management

Thesis directed by Professor John Pellegrino

This research focuses on the evaluation of factors in the design of a static mixer crystallizer to induce crystallization in supersaturated brine streams. Current brine management systems are unsatisfactory in inland contexts, limiting the economic feasibility of inland desalination. For inland desalination to become feasible it is essential for water recovery to increase and the cost of brine disposal to be reduced. Inducing crystallization in brine works towards both those problems by removing salts, allowing the brine solution to be filtered again. The static mixer investigated in this work has the potential to be energy and cost efficient without the need for chemical additions. To evaluate design parameters, brine solutions are modeled by mixing two solutions together to create a supersaturated solution that is pumped through the static mixer. The resulting turbidities, solids in solution, and calcium ion concentrations are then measured. Factors evaluated include the shape of the 3-d printed mixer inserts, material of mixer inserts, nominal residence time, and diameter and length of the static mixer. The results show that one shape, rotelle, performs worse than the other three shapes, and suggest that one material, polyethylene terephthalate glycol, performs better than the other two evaluated. However, high variability and lack of reproducibility in results limited the conclusions that can be drawn from the data. As a result of this variability, much of the focus of this research is on developing an

improved experimental procedure and methodology. Future work using this improved procedure is needed to fully evaluate all the design parameters.

## **Dedication**

To Joe Guinasso, who lifted those around him

## **Acknowledgements**

I would like to thank my entire family, for without them none of this would have been possible. I thank Wendy Shelton, Mike Montgomery, Darren Moss, Jeff Serling, Bob Richardson, Steve Kingma, Jeff Higgins, John Throckmorton, Eric Peterson, Dr. Jeff Cannon, Dr. Don Rodrigues and Professor Anne Yu for all the support I have received over the years. I thank Dr. Pellegrino for the opportunity to perform this research and for his guidance. I thank Mr. Saied Delagah of the Bureau of Reclamation for his support of this project. I thank Dr. Julie Korak for ICP-MS analysis, as well as being part of my committee. Finally, I thank Dr. Joe Ryan for being part of my committee.

## Contents

Chapter 1 – Introduction .....	1
1.1 Motivation for research .....	1
1.2 Static mixer background .....	5
1.3 Crystallization theory .....	6
1.4 Previous work .....	8
Chapter 2 – Methods .....	10
2.1 Initial experimental procedure .....	10
2.2 Determining Viable Model Solution .....	24
2.3 Improving sampling procedure .....	29
Chapter 3 – Results and discussion .....	36
3.1 Raw experimental results .....	36
3.2 Data analysis .....	39
3.3 Discussion .....	61
Chapter 4 – Conclusion .....	68
4.1 Conclusion .....	68
4.2 Future work .....	69
Bibliography .....	74
Appendix A – Summary of procedures .....	79
Appendix B – Prepared solution disequilibrium .....	80
Appendix C – Additional Kolmogorov mixing lengths .....	97
Appendix D – Residence time distributions .....	99

## List of Tables

Table 1 - Chemical inputs for the two constituent solutions of solution 1 .....	14
Table 2 - Chemical inputs for the two constituent solutions of solution 3 .....	27
Table 3 - Chemical inputs for the two constituent solutions of solution 4 .....	28
Table 4 - Chemical inputs for the two constituent solutions of solution 5 .....	29
Table 5 - Summary of experiments run at 48” length, 0.5” diameter, and solution 5 for both the inflow apparatus constructed with two T-junctions and three T-junctions .....	32
Table 6 - Chemical inputs for the two constituent solutions of solution 6 .....	34
Table 7 - Table showing saturation index and which salt species are supersaturated for the six solutions used in this work .....	35
Table 8 - Experimental results for all experiments run using procedure 1 .....	37
Table 9 - Experimental results for all experiments run using procedures 2 and 3 .....	38
Table 10 - Table showing the factors and levels for experiments ran using solution 5, at 0.5” diameter, and 48” length .....	49
Table 11 - Table showing the factors and levels for experiments ran using solution 5, at 0.5” diameter, 48” length, and PETG .....	51
Table 12 - Table showing the factors and levels for experiments ran using solution 5, at 0.5” diameter, 96” length, and PETG .....	52
Table 13 - Table showing the factors and levels for experiments run using solution 5, at 0.5” diameter, and PETG .....	53
Table 14 - Table showing the factors and levels for experiments ran at an 11 min residence time, using solution 5, at 1” diameter, and 48” length .....	54
Table 15 - Table showing the factors and levels for experiments ran at an 11 min residence time, using solution 5, PETG, and 48” length .....	55
Table 16 - Number of experiments for each combination of shape and residence time using solution 5, at 0.5” diameter, 48” length, and PETG .....	57
Table A1 - Summary of the three procedure used in this work .....	80
Table B1 - Experiments conducted at 1” diameter, shape of Farfalle, material of PETG, 48” length, 11-minute residence time, and solution 11 .....	82
Table B2 - Experiments conducted at 1” diameter, shape of Hourglass, material of PETG, 48” length, 11-minute residence time, and solution 11 .....	83
Table B3 - Components of proposed new solution .....	91

Table B4 - Resulting concentrations of select ions in new solution, calculated from OLI simulation and literature values for brine from site 1 .....91

Table B5 - Results of benchtop experiment combing aliquots of solution 5A with 5B, then measuring turbidity after time .....94

Table B6 - Results of benchtop experiment combing aliquots of the solutions shown in table B3 with variable amounts of NaOH added, then measuring turbidity after time .....95

Table D1 - Variance and skewness for a step input residence time distribution at a 7 min nominal residence time, 1” diameter and 48” length tubing, using conductivity to measure the concentration of a NaCl solution .....100

## List of Figures

Figure 1 - Farfalle static mixer inserts at 1" and ½" diameter .....	11
Figure 2 - Rotelle static mixer inserts at 1" and ½" diameters .....	12
Figure 3 - Shell static mixer inserts at 1" and ½" diameters .....	12
Figure 4 - Hourglass static mixer inserts at 1" and ½" diameters .....	13
Figure 5 - The two 50 L tubs with stir sticks used for all experiments .....	16
Figure 6 - The tubing set up including the intermediate tubing to bridge the size gap .....	18
Figure 7 - Initial static mixer inflow setup for 0.5" diameter mixer .....	19
Figure 8 - Static mixer outflow setup for 0.5" diameter tubing .....	20
Figure 9 - Example of the rotation used for farfalle inserts .....	21
Figure 10 - Example of the rotation used for shell inserts .....	21
Figure 11 - Full static mixer apparatus for 0.5" diameter tubing .....	22
Figure 12 - Side by side comparison of old and new experimental apparatus setups .....	30
Figure 13 - Schematic of sample filtration apparatus .....	31
Figure 14 - Results of a 2-sample Kolmogorov-Smirnov tests examining resulting turbidities at 90 min for five distinct sets of parameters for both experimental apparatus', using two and three inflow T-junctions .....	33
Figure 15 - A plot of total depletion and turbidity for experiments at 1" diameter, 48" length and solution 5 .....	40
Figure 16 - A plot of solids collected and turbidity for experiments at 1" diameter, 48" length, solution 5 and procedure 2 .....	42
Figure 17 - A plot of solids collected and turbidity for experiments at 1" diameter, 48" length, solution 6 and procedure 3 .....	42
Figure 18 - Average turbidities at 60 min for each set of parameters with data at 0.5" diameter, PETG, 48" length and solution 1 plotted against Kolmogorov mixing length .....	44
Figure 19 - Average turbidities at 60 min for each set of parameters with data at 0.5" diameter, PETG, 48" length and solution 5 plotted against Kolmogorov mixing length .....	44
Figure 20 - Average turbidities at 60 min for each set of parameters with data at 0.5" diameter, PETG, 96" length and solution 5 plotted against Kolmogorov mixing length .....	45
Figure 21 - Average turbidities at 90 min for each set of parameters with data at 1" diameter, PETG, 48" length and solution 5 plotted against Kolmogorov mixing length .....	45

Figure 22 - Turbidities at 60 min plotted against shape and residence times for PETG, 48” length, solution 1 and 0.5” diameter .....47

Figure 23 - Average turbidities at 60 min plotted against shape and residence times for PETG, 48” length, solution 5 and 0.5” diameter .....48

Figure 24 - 3-way ANOVA test examining interactions between shape, material, and residence time on turbidities at 60 min for experiments ran using solution 5, at 0.5” diameter, and 48” length .....49

Figure 25 - Results of two-sample Kolmogorov–Smirnov test comparing turbidities at 60 min for PETG and PC for solution 5, 0.5” diameter, 48” length, 7 min residence time and shell .....50

Figure 26 - 2-way ANOVA test examining interactions between shape and residence time on turbidities at 60 min for experiments ran using solution 5, at 0.5” diameter, 48” length, and PETG .....51

Figure 27 - 2-way ANOVA test examining interactions between shape and residence time on turbidities at 60 min for experiments ran using solution 5, at 0.5” diameter, 96” length, and PETG .....52

Figure 28 - 3-way ANOVA test examining interactions between shape, tubing length and residence time per 48” length on turbidities at 60 min for experiments run using solution 5, at 0.5” diameter, and PETG .....53

Figure 29 - 2-way ANOVA test examining interactions between shape and material on turbidities at 90 min for experiments ran at an 11 min residence time, using solution 5, at 1” diameter, and 48” length .....55

Figure 30 - 2-way ANOVA test examining interactions between shape and diameter on turbidities at 60 min for experiments ran at an 11 min residence time, using solution 5, PETG, and 48” length .....55

Figure 31 - 2-sample Kolmogorov-Smirnov tests comparing turbidity at 60 minutes for rotelle and farfalle for experiments ran using solution 5, at 0.5” diameter, 48” length, and PETG .....58

Figure 32 - 2-sample Kolmogorov-Smirnov tests comparing turbidity at 60 minutes for rotelle and shell for experiments ran using solution 5, at 0.5” diameter, 48” length, and PETG .....58

Figure 33 - 2-sample Kolmogorov-Smirnov tests comparing turbidity at 60 minutes for rotelle and hourglass for experiments ran using solution 5, at 0.5” diameter, 48” length, and PETG .....59

Figure 34 - 2-sample Kolmogorov-Smirnov tests comparing the turbidity at 90 minutes for PETG and PP for experiments ran with an 11 min residence time using solution 5, at 1” diameter, and 48” length .....60

Figure 35 - 2-sample Kolmogorov-Smirnov tests comparing turbidity at 90 minutes for PETG and PC for experiments ran with an 11 min residence time using solution 5, at 1” diameter, and 48” length .....60

Figure 36 - 2-sample Kolmogorov-Smirnov tests comparing the turbidity at 90 minutes for PP and PC for experiments ran with an 11 min residence time using solution 5, at 1" diameter, and 48" length .....	61
Figure B1 - pH over time for 6 L of solution 5A left open to atmosphere .....	85
Figure B2 - pH over time for 6 L of solution 5B left open to atmosphere .....	86
Figure B3 - pH over time for 12 L of solution 5A left open to atmosphere .....	87
Figure B4 - pH over time for 12 L of solution 5B left open to atmosphere .....	87
Figure B5 - Water composition data taken from brine solutions collected at various inland sites in Southern California .....	90
Figure B6 - Measured turbidities after different times for aliquots of solution 5 and the new solution shown in table B3 and 0.1375 g/L NaOH .....	96
Figure C1: Average turbidities at 60 min for each shape with data using a 3 min residence time, at 0.5" diameter, PETG, 48" length and solution 5 plotted against Kolmogorov mixing length .....	98
Figure C2: Average turbidities at 60 min for each shape with data using a 7 min residence time, at 0.5" diameter, PETG, 48" length and solution 5 plotted against Kolmogorov mixing length .....	98
Figure C3: Average turbidities at 60 min for each shape with data using a 11 min residence time, at 0.5" diameter, PETG, 48" length and solution 5 plotted against Kolmogorov mixing length .....	99
Figure C4: Average turbidities at 60 min for each shape with data using a 11 min residence time, at 0.5" diameter, PETG, 48" length and solution 5 plotted against Kolmogorov mixing length .....	99
Figure D1: F(t) plot for the RTD of shell at a 7 min nominal residence time, 1" diameter and 48" length tubing .....	100
Figure D2: F(t) plot for the RTD of rotelle at a 7 min nominal residence time, 1" diameter and 48" length tubing .....	101
Figure D3: F(t) plot for the RTD of farfalle at a 7 min nominal residence time, 1" diameter and 48" length tubing .....	101
Figure D4: F(t) plot for the RTD of hourglass at a 7 min nominal residence time, 1" diameter and 48" length tubing .....	102

## List of acronyms

ICD= intermediate concentrate treatment

NTU= nephelometric turbidity units

DI= deionized

CSTR= completely stirred tank reactor

$\eta$ = Kolmogorov mixing length scale

$\nu$ = kinematic viscosity of a solution

PETG = polyethylene terephthalate glycol

PC = polycarbonate

PP = polypropylene

ICP-MS = inductively coupled plasma mass spectrometry

PVC = polyvinyl Chloride

IAP = ionic activity coefficient

SI = saturation index

## Chapter 1

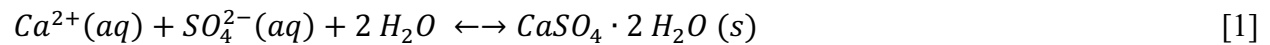
### 1.1 Motivation for research

An adequate supply of water is essential for economic, societal, and human development and health<sup>1</sup>. Water availability is highly dependent on location, and water is difficult to transport over long distances, meaning local water resources are almost always drawn upon for supply in each location. In many locations and regions, water supplies have historically been, or are currently being drawn from unsustainably. Dwindling supplies of water that is high quality, unpolluted and with low electrolyte concentrations have made purification of lower quality water increasingly economically feasible<sup>1-3</sup>. Brackish (lower in electrolytes and total dissolved solids than seawater, but too high to be used without purification for many applications) water sources such as lower quality aquifers, domestic and industrial wastewaters, and agricultural runoff are all water sources that require purification that have traditionally not been fully utilized<sup>4</sup>. One method of purification is pressure driven membrane-based water purification, such as reverse osmosis membrane filtration. Since this thesis will focus on reverse osmosis filtration of solutions high in sparingly-soluble electrolyte salts, this method will be referred to as desalination. Though there are downsides to this form of desalination, such as high energy requirements, high levels of initial capital required, and high upkeep costs, the two largest problems are efficiency and brine management<sup>2</sup>. Brine, or retentate solutions, are typically handled in coastal desalination situations by diluting with seawater and releasing it into the ocean. Though there are environmental impacts, with the severity varying on the local context and the exact specifications of disposal, brine disposal in these coastal plants is very rarely the major barrier to economic viability<sup>2,5</sup>. However, in inland desalination contexts, all the current methods for dealing with brine streams, including deep well injection, evaporation ponds, and transportation to the sea,

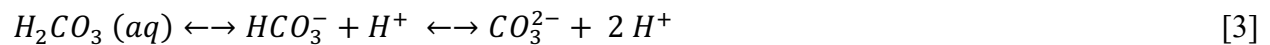
have major problems with either cost or environmental impacts, or both<sup>5-7</sup>. For example, deep well injection requires extensive research and permitting before beginning operations, and an appropriate geological formation to inject into. Appropriate permitting is increasingly difficult to acquire as concerns over groundwater contamination and other environmental impacts grow<sup>4</sup>. Transportation of brine over even short distances to the injection wells is difficult and costly due to the volume of brine transported and precipitated solids in the line creating issues<sup>3</sup>. Furthermore, all of methods are limited by the volume of brine solution that can effectively be treated in one location and fail to scale upwards feasibly<sup>2</sup>. One emerging technology, solar crystallizers, are receiving significant interest and study, and have shown promising results<sup>8-11</sup>. However, no technoeconomic assessments currently exist for this technology, and major concerns with scalability remain.

Another problem facing inland desalination is low efficiency of purification. Though it varies greatly based on the specific system and the characteristics of inflow solution, the retentate solution can account for anywhere from 5-70% of the volume of inflow<sup>5</sup>. In the context of where many of these inland desalination systems are implemented, water scarcity is a major concern, and this low level of efficiency limits the effectiveness and economic feasibility of these systems. In many cases, the limit in recovery is governed by the composition of the feed solution. When the brine solution reaches a concentration where scaling, or solids formed along a surface, begins to occur along the membrane, flux through that membrane drops and operating costs increase<sup>12,13</sup>. Therefore, it is important to limit the water recovery of a system to the point where the brine solution is not fouling the membranes. To increase the water recovery of desalination systems, chemical antiscalants are added to feed solutions, which increase the amount of water recovery and by extension the concentration of salt species in the brine that can be achieved

without scaling and fouling the membrane<sup>14</sup>. As a result, in many cases, the brine solutions are supersaturated for one or more chemical species. These species are categorized as sparingly soluble salts due to their low solubilities. Though the exact chemical species that limits water recovery can vary depending on the exact composition and source of feed water, the two most common and important salts are calcium carbonate ( $\text{CaCO}_3$ ), in the form of calcite, and calcium sulfate, in the form of gypsum ( $\text{CaSO}_4 \cdot 2 \text{H}_2\text{O}$ )<sup>3,15,16</sup>. The precipitation of gypsum follows equation 1.



While gypsum precipitation is relatively straightforward, calcite is governed by a more complex set of stoichiometric speciation equations.



One important note is that the total carbonate in a system that is open to the atmosphere is variable, with  $\text{CO}_2$  dissolving into a system through equation 2 lowering the pH as the  $\text{H}_2\text{CO}_3$  dissociates through equation 3. Conversely,  $\text{CO}_2$  being released into the atmosphere raises the pH through the opposite mechanism. Another important consequence of these governing equations is that although the precipitation of calcite shown in equation 4 does not include  $\text{H}^+$  or  $\text{OH}^-$  directly, the process is highly pH dependent as the proportion of total carbonate in the form of  $\text{CO}_3^{2-}$  needed to react to form calcite, governed by equation 3, depends strongly on pH. These three equations combine to form a dynamic equilibrium.

A method for addressing the problems facing inland desalination, low water recovery and high brine management costs, is to allow or induce the precipitation of salt solids in the brine solution, then separate the solids from it. The saturated brine solution can then be processed through a second desalination process to increase water recovery. The water that would ordinarily have been stuck in supersaturated brine solution can then be recovered, theoretically allowing a much higher level of efficiency. The salts, now in solid form instead of being dissolved in a brine solution, are then easier and cheaper to transport and dispose of. This general method is known as intermediate concentrate demineralization, or ICD. Furthermore, in certain contexts, these salts are economically valuable, and their recovery and sale can be used to offset some of the operation and maintenance costs of a desalination plant<sup>1,2</sup>.

Extensive work has been done to design and evaluate different methods for inducing precipitation in brine solutions to increase water recovery<sup>15-23</sup>. Many of these methods follow a two-step process, though almost all investigated methods use some combination of the two following concepts. First, the supersaturation of calcite is raised by increasing the pH of the solution, increasing the proportion of total carbonate in the form of  $\text{CO}_3^{2-}$  as shown in equation 3, either by adding lime,  $\text{Ca}(\text{OH})_2$ , or soda ash,  $\text{Na}_2\text{CO}_3$ . This increase in supersaturation usually induces crystal formation, which subsequently provide a surface for antiscalants present to adsorb to, removing or “scavenging” the antiscalants from the solution<sup>18</sup>. After the antiscalant has been removed, gypsum precipitation can then be induced by adding seed crystals, or small gypsum crystals that provide an anchor and nucleation surface for further crystal growth. This is known as chemically-enhanced seeded precipitation, or CESP. Though these processes are promising, particularly for application in agricultural drainage purification, they are, for the moment, not economically feasible to implement<sup>18</sup>. Economic assessment of CESP is difficult

due to the highly variable nature of composition of agricultural drainage and the market value of purified water, but two major barriers for CESP are increased operation and maintenance costs compared to traditional, one stage, reverse osmosis, and the cost of chemical inputs. The main motivation for this research is to develop a method for inducing crystallization in brine for ICD that does not require additional chemical inputs, and to investigate the effect of mixing energies and material surface topologies on crystallization of sparingly soluble salts.

Previous work looking into inducing precipitation in brine solutions using only mechanical action investigated CSTRs-in-series as an approach and found that though more investigation is needed, the CSTR-in-series were able to increase the rate of crystallization without the need for additional seed crystals or other inputs<sup>24</sup>. Based on these findings, static mixers were identified as a potentially more efficient (compact) method of inducing crystallization versus CSTRs-in-series.

## **1.2 Static Mixer Background**

A static mixer is a series of non-moving pieces or inserts that are placed inside a pipe or reactor that change the flow pattern by redistributing flow and creating turbulence<sup>25</sup>. Specific inserts alter the flow in different ways, and different applications have different inserts. In industry, static mixers are commonly used for thorough mixing between two streams, though they can provide other functions depending on the application. Static mixers have a number of distinct advantages over other reactor or mixing set ups due to low operational costs, as energy is only needed for pumping, a compact and space efficient design, and low up front equipment costs<sup>25</sup>. In addition to these general advantages for various industrial uses, static mixers have some specific characteristics that align well with designing a reactor to induce precipitation. First, similar to CSTRs-in-series, the solution will continuously have mixing energy imparted into the

system. It is this similarity that provides the theoretical justification for the possibility that the previously mentioned positive results found from using CSTRs-in-series will also be seen in static mixers. Next, the variety of parameters such as flow rate, energy dissipation, size of the mixer, and shape and material of the static inserts, provides customizability and the ability to create the exact fluid dynamic conditions necessary to maximize the rate of crystallization. Additionally, the static inserts can greatly increase the surface area inside the mixer, providing points for heterogenous nucleation, a concept that will be expanded upon in the next paragraph. Finally, the ability to remove the inserts from the pipe housing the mixer will allow easier maintenance and cleaning, which is not an insignificant factor when dealing with precipitation processes. This combination of potentially increased efficiency, and an increase in the number of factors and conditions that can be examined led to the switch from CSTRs-in-series to an inline static mixer.

### **1.3 Crystallization Theory**

According to classical theory, crystallization occurs in two distinct phases: nucleation and growth<sup>26-28</sup>. During nucleation, an infinitesimally small group of molecules overcome the energy barrier required to change phases, in this case from liquid to solid. In classical theory, the free energy of nucleation is calculated by adding the free energy requirement to change the phase of a given number of molecules to the free energy from those molecules being removed from the solution, therefore decreasing the concentration of the crystallizing species in solution<sup>26,27</sup>. The free energy of removing a species from solution is negative when the concentration of that species is higher than equilibrium concentration, or when the solution is supersaturated for a particular species. The energetic favorability of moving to equilibrium concentration is therefore the driving force behind nucleation. Though any supersaturated solution will energetically favor

crystallization until equilibrium concentration is reached, the substantial free energy cost of initial nucleation (the positive free energy change involved in creating surface area of a growing crystal) and the degree of supersaturation in solution govern the kinetics of nucleation<sup>29</sup>. For a given chemical species and conditions such as pressure and temperature, there is a range of concentrations of ions in solution where the solution is supersaturated, and will eventually form precipitate, but is below the concentration where this precipitation is instantaneous because of the energy requirements of nucleation<sup>30</sup>. This “zone”, or range of concentrations, is known as the metastable zone. Therefore, the goal of the static mixer crystallizer is to increase the number of collisions per unit volume in supersaturated, metastable solutions and increase the rate of nucleation and growth (see next paragraph) enough to lower the ion concentrations to the bottom of the metastable zone, more quickly, resulting in total de-supersaturation.

In the growth phase, the supersaturated species precipitates in layers outwards from the initial small cluster<sup>28,31</sup>. At small sizes, the free energy of these crystallized clumps is increased by a term guided by surface area, with increasing surface area being unfavorable, and a term guided by volume, with increased volume being favorable<sup>26</sup>. The overall energetic favorability of a small crystal growing is therefore guided by the ratio of surface area to volume of the crystal. There exists a crystal size, known as the critical size, with a certain surface area to volume ratio, in which the addition or removal of one molecule is equally likely. If a molecule of this critically sized cluster dissolves, the cluster drops below this critical size, surface area dominates, and it is overwhelmingly likely that the full cluster dissolves. If a molecule is added to the critically sized cluster, it is raised above the critical size, volume dominates, and it is overwhelmingly likely that the cluster grows.

There are two forms of nucleation: homogeneous and heterogeneous. In homogeneous nucleation, the incipient crystal forms in bulk solution, in a roughly spherical shape. In heterogeneous nucleation, the crystal begins attached to a foreign surface, usually the walls of the vessel, a contaminating solid particle, or an existing crystal above critical size introduced to the solution called a seed crystal<sup>32</sup>. Of the two, heterogeneous nucleation dominates, as building upon a solid surface allows the portion of the crystal directly attached to the surface to be shielded from the solution, and therefore decrease the surface area to volume ratio. The use of a static mixer can greatly increase the heterogeneous surface area in which crystals can nucleate and achieve critical size. An ideal static mixer will therefore allow crystals to nucleate and grow to critical size attached to the surface of the inserts, then be detached from the surface by fluid dynamic conditions where it can continue to grow in bulk solution. Finally, these growing crystals must not be allowed to settle out of solution until leaving the static mixer for the maximum efficiency.

#### **1.4 Previous work**

Static mixers have been used to induce crystallization in pharmaceutical and other low throughput, high value chemical production, where the primary concerns are efficiency, cost and low variability in crystal size and morphological characteristics<sup>33–37</sup>. The impetus for much of this work is to convert from batch crystallization processes to a continuous crystallization process, which is theoretically more efficient, scalable and cost effective<sup>29,38,39</sup>. Research into static mixer use for crystallization of bulk electrolytes is limited, with the exception of a 2019 paper that investigated using two commercially available static mixers for precipitating CaF<sub>2</sub> from a supersaturated solution<sup>40</sup>. That study found static mixers to be effective at inducing precipitation, but the paper was primarily focused on the theoretical underpinnings of

crystallization, rather than designing or evaluating a static mixer for high throughput crystallization, and no further work has followed.

In this thesis, static mixer inserts of various shapes and constructed from various polymers are investigated. 3-d printing is used to produce the inserts as a low-cost production method of producing pieces with customized shapes in small quantities<sup>41</sup>. Due to these desirable characteristics, extensive research has been undertaken investigating the use of 3-d printing for production of static mixer inserts<sup>42-46</sup>. Most of these static mixers are printed using some kind of metal, then coated with a substance to gain the desired surface chemistry for use as a reactor. In contrast, the inserts used in this thesis are printed directly from various polymers.

The use of polymers and the effect of their specific surface chemistries in crystallization is a topic that has recently been the subject of significant study<sup>47</sup>. The functional groups on the polymer face, the topography of the surface or form of polymer microstructures and the surface chemistry of a polymer have all been topics of interest in recent papers, with a demonstrated correlation between all these characteristics and the rate of nucleation and growth kinetics<sup>48-53</sup>. Unfortunately, these studies are mostly empirical studies, and theory-driven, rational design of polymers for specific purposes (either inhibiting or promoting crystal formation and growth, or promoting a specific crystal polymorphism) are limited by a lack of understanding of the specific mechanisms guiding crystal formation<sup>54</sup>. As a result, several different polymers are tested in this paper to determine which has the best performance in this application. Three polymers investigated are widely used in 3-d printing, and available commercially in the form of industrially produced filaments: polyethylene terephthalate glycol (PETG), polycarbonate (PC), and polypropylene (PP).

## Chapter 2

### 2.1 Initial experimental procedure

For this work, four different insert shapes are investigated. The first three mixer element designs were based on common pasta shapes. This was due to the desire to study a diverse set of inserts that provide a range of parameter values. The fourth design shape, hourglass, was designed to mimic the hydrodynamic effect of a peristaltic pump, due to the suggestion from the work looking at CSTRs-in-series that the use of peristaltic pumping was aiding the rate of crystallization<sup>24</sup>. A peristaltic pump creates conditions in the flow of alternating high pressure and low-pressure packets of solution, which is likely emulated by the design of the hourglass inserts. All insert pieces are 3-d printed using an Original Prusa i3 MK3S+ printer. Printed farfalle, rotelle, shell and hourglass pieces of various materials and 0.5” and 1” diameter are shown in figures 1-4.



*Figure 1: Farfalle static mixer inserts at 1" and 1/2" diameters.*

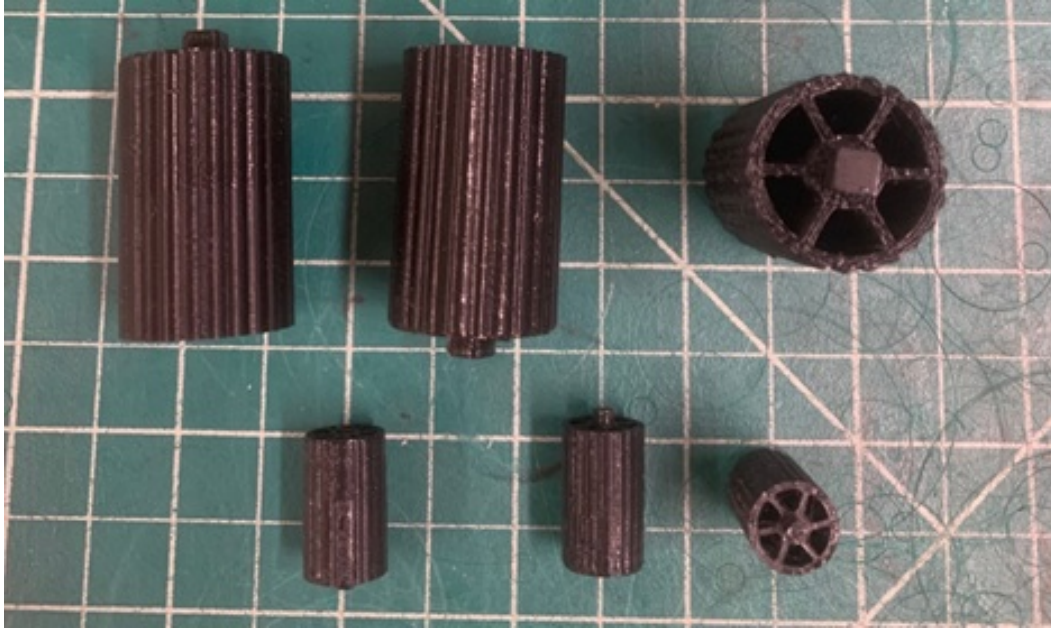


**Figure 2:** Rotelle static mixer inserts at 1" and 1/2" diameters.



**Figure 3:** Shell static mixer inserts at 1" and 1/2" diameters.

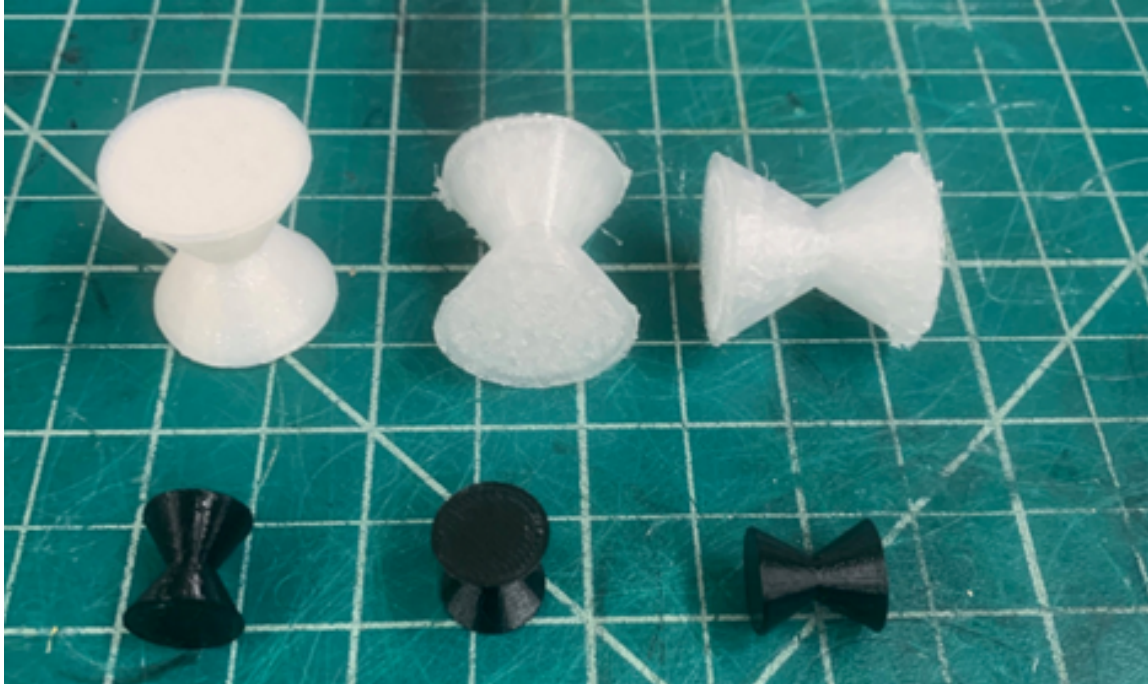


**Figure 4:** Hourglass static mixer inserts at 1" and 1/2" diameters.

From previous work done in the group, several elements of experimental design were already in place, including the idea of 3-d printed static mixer pieces, the four shapes themselves, and the initial materials for the inserts. Also decided was an experimental set-up involving using peristaltic pumps to mix two solutions together, that, when mixed, are supersaturated for at least one chemical species. This supersaturated solution is pumped through the static mixer and measured for turbidity. The final major experimental parameter was residence time. For this, 3, 7 and 11 minutes were selected somewhat arbitrarily to provide a wide range of flow rates to test. Adjustments and improvements to procedure and methodology made over the course of these experiments are detailed in a later section, while this section details the procedure at the start of research studies (aka initial experiments).

To begin, two solutions are prepared. The chemical inputs of these initial solutions are shown in table 1. The resulting, mixed solution from these two constituent solutions will be referred to as “solution 1”.

**Table 1:** Chemical inputs for the two constituent solutions of solution 1.

constituent	solution 1A	solution 1B
H <sub>2</sub> O (L)	0.5	0.5
CaCl <sub>2</sub> (anhydrate) (g)	1.4760	0
MgSO <sub>4</sub> (heptahydrate) (g)	1.2264	0
Na <sub>2</sub> SO <sub>4</sub> (g)	0	1.5624
NaHCO <sub>3</sub> (g)	0	1.5624

This solution had been used in previous work in the group and was based on data from the brine composition of a Brighton, CO desalination plant, chosen as a representative composition of the brine produced at the kind of plants this work is targeting<sup>24,52</sup>. The use of this composition further maintains continuity between this work and all concentrate management work done previously in the group, providing some baseline data for the crystallization kinetics and properties of a solution produced with this composition.

One useful tool to help understand solution composition are saturation indexes. A saturation index is a way to quantify the relationship between the activity of components of a particular chemical species in solution at a given time, and the activity of those components at equilibrium. While many different equations for calculating a saturation index exist, this thesis will use the

form shown in equation 5, where  $IAP_x$  refers to the ion activity product and  $Ksp_x$  refers to the solubility activity product for a given salt species  $x$ <sup>16,55</sup>.

$$SI_x = IAP_x / Ksp_x \quad [5]$$

This solution, when combined, at a theoretical instantaneous moment where no precipitation has occurred, has a saturation index for calcite ( $SI_c$ ) of 764. The solutions were prepared by calculating the salt masses needed for a targeted total volume. The  $CaCl_2$  is then weighed into an appropriately sized beaker. A 2L beaker is then obtained, filled with around 2 L of DI water, placed with a stirring rod on a stir plate and turned on. The  $CaCl_2$  was then poured into this 2 L beaker, with any visible residue washed into the 2 L beaker with DI water. A clearly marked 50 L tub with stir stick is then obtained, shown in figure 5.



**Figure 5:** The two 50 L tubs with stir sticks used for all experiments, unless noted otherwise.

This tub had its mass taken and recorded, then rinsed with DI water three times, and placed on a scale. The beaker that had contained the  $\text{CaCl}_2$  is then rinsed once more with DI water into the tub. Next the necessary  $\text{MgSO}_4$  is weighed into an appropriately sized beaker. When the  $\text{CaCl}_2$  has fully dissolved, and there are no visible crystals or turbidity, this solution is poured into the tub on the scale. The beaker is washed twice with DI water into the tub, once with the stir rod still in place, and once with it removed. This beaker is then filled once more with 2 L of DI water

and placed back on the stir plate with the stir bar. The  $\text{MgSO}_4$  is then poured into this 2 L beaker, with the  $\text{MgSO}_4$  beaker being rinsed twice, once into the stirred beaker, and once into the tub on the scale. When the  $\text{MgSO}_4$  is fully dissolved, this solution is poured into the tub and washed twice, once with the stir bar and once without. DI water is then added to the tub until the desired volume is achieved. The solution is then stirred with the stirring stick. Depending on the volume of solution, either a short amount of spinning, around 30 seconds, or a longer time alternating between spinning and a canoe paddle like action to mix vertically is necessary. This solution is then set aside with the lid slightly open. All glassware is cleaned with soap and water, and the same procedure is followed to produce the second solution, only with  $\text{Na}_2\text{SO}_4$  and  $\text{NaHCO}_3$  being added instead of  $\text{CaCl}_2$  and  $\text{MgSO}_4$ .

The first experiments were run using 0.5" diameter polyvinylchloride (PVC) pipe as the static mixer housing, and the necessary flow rates were never more than 1 mL/s, so preparing two 6 L solutions, for a total of 12 L mixed solution became standard. This was the lowest volume that allowed the two salts for each solution to be dissolved into their own 2 L beaker, and enough room to fully wash the beaker both times.

After both solutions are prepared and stirred, they are left with the lid open overnight, so that they have 16-24 h to equilibrate with atmospheric gasses, particularly  $\text{CO}_2$ . The importance of this exchange is shown in equations 2, 3, and 4, and discussed in the paragraph these equations appear. This portion of the procedure was already defined by previous work within the group, and will be discussed in detail later as it proved to be a step in the procedure that contributed to high variability in later experiments.

After the solutions have sat overnight exchanging gasses with the atmosphere, the experimental apparatus is assembled. For the feed lines, 3/8" diameter ClearFlex PVC tubing is connected to

MasterFlex 0.03” diameter tubing, then fed into a MasterFlex L/S easy load II peristaltic pump. To bridge the size gap between the two tubes, 1/16” diameter Finger Lakes Extrusion Clearflex PVC tubing is inserted inside the 3/8” tubing, and secured with a fitting, while the 0.03” tubing is inserted inside the 1/16” tubing and secured with copper wire as shown in figure 6. The wire is used to create an airtight seal between the differently sized tubing.



*Figure 6: The tubing set up including the intermediate tubing to bridge the size gap.*

Before the other end of 1/16” PVC tubing is connected to more 3/8” diameter ClearFlex PVC tubing, the flow rates are tested and calibrated. To perform this calibration, a bucket is filled with DI water and the leads are inserted. The pump is then run until both tubes are totally full, then the pump is turned off. The ends of the two outflow 1/16” PVC tubing are then placed in empty beakers, and the pump is then run for a desired length of time, usually between 3-5 min. The volume of water in the two beakers is measured, and if they are different by more than 2.5%, the tubing is adjusted by tightening or loosening the wire ties, or the tightness of the peristaltic pump. This is repeated until the flow rates are within 2.5%, at which point the tubes are fully drained, and the inline mixer is prepared.

The inline mixer consists of two lengths of 3/8” diameter ClearFlex PVC tubing connected to two barbs attached to a 0.5” diameter PVC T-junction, as shown in figure 7.



**Figure 7:** Initial static mixer inflow setup for 0.5" diameter mixer.

This inflow T-junction is then connected to a second T-junction. This second T-junction is connected to a valve with a hose barb, and 48" length, 0.5" diameter clear PVC pipe. The outflow end of this tubing is again attached to a 0.5" diameter PVC T-junction as shown in figure 8.



**Figure 8:** Static mixer outflow setup for 0.5" diameter tubing.

This T-junction has two hose barbs attached to it. From one barb, more clear 3/8" diameter ClearFlex PVC tubing leads to a valve for outflow. A Cole Parmer pressure transmitter has 3/8" diameter ClearFlex PVC tubing leads attached to both ends, with one connecting to the remaining barb at the static mixer inflow, and one attached to the remaining barb at the outflow.

Though the shape and material of the inserts change depending on the parameters of a particular experiment, to help hold the pieces being targeted in place, three farfalle PETG pieces are placed in the inflow T-junctions, while two farfalle PETG pieces are placed in the outflow T-junction. These pieces are included to ensure the main static mixer pieces remain inside the main static mixer pipe to reduce variability and to prevent pieces from becoming lodged in the T-junctions. Finally, the main tubing is filled with the static mixer elements of the shape and material being targeted in that experiment. Since hourglass shaped inserts have no interlocking mechanism, hourglass inserts are loaded into the pipe end to end. For rotelle shaped inserts, the pieces are added one by one taking care to insert the square shaped key of one piece into the square shaped lock of the preceding piece, so that no rotation can occur by individual pieces. For farfalle inserts, the pieces are added like rotelle except each piece is rotated 90 degrees either direction from the previous piece, as shown in figure 9.



**Figure 9:** Example of the rotation used for farfalle inserts.

For shell, each piece is rotated 90 degrees clockwise from the previous piece, as shown in figure 10.

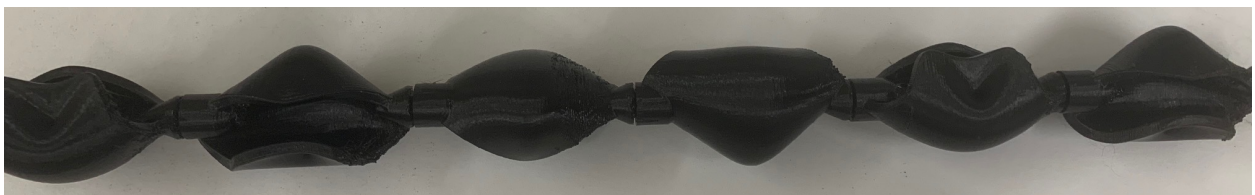


**Figure 10:** Example of the rotation used for shell inserts.

Though an attempt is made to always follow these rotation patterns, when loading the inserts occasionally two pieces will disconnect when already in the main pipe and it is not always possible to reattach them with the correct rotation, causing a disruption in the pattern. In these cases, if there are more than three discontinuities, the pieces are unloaded and loaded again, while if there are only one or two breaks, the experiment is run anyways.

The main static mixer pipe is then attached to the inflow and outflow T-junctions and placed at a 7-degree angle to minimize the air bubbles that will be caught in the mixer.

The resulting, completed apparatus is shown in figure 11.



**Figure 11:** Full static mixer apparatus for 0.5" diameter tubing.

Using this apparatus, crystallization experiments are conducted. A crystallization experiment is begun by stirring the prepared solutions vigorously (usually around 30 s for 6 L batches, longer for higher volumes), then inserting the pump leads into the stirred solutions. The peristaltic pump is then turned on at the desired RPMs. As the tubing fills with solution, the tubing is manipulated to ensure no air bubbles are trapped in the line that can release during the course of the

experiment. When the leading edge of the solution is visible in the main pipe, a timer is started. This time is stopped when the leading edge of the solution has passed beyond the main pipe into the outflow T-junction. This residence time is used to help align flow rates and pump RPMs to residence time and ensure that nothing has gone wrong with the pump, rather than for subsequent calculations. When the solution begins to flow from the outflow tubing, the time is marked. Measurements are then taken every 5 min. A measurement consists of using a Hach Portable Turbidimeter Sample Cell being filled to the appropriate mark from the solution outflow, approximately 80% full, and a reading being taken using a Hach Portable Turbidimeter. A conductivity and temperature reading of the outflow is taken using a Myron L Company Ultrameter II conductivity probe, and pressure drop reading is taken using a Cole Parmer differential pressure transmitter. For the first set of experiments, this set of measurements is taken until the turbidity is consistently below 3 nephelometric turbidity units (NTUs), or 60 min has passed, unless the turbidity has not leveled off after 60 min, in which case measurements are taken until the turbidity does level off or 90 min is reached.

The purpose of these experiments is to determine the effectiveness of a certain set of parameters in inducing precipitation of solids from a supersaturated solution, so the ultimate figure-of-merit is the static mixers performance in decreasing the degree of supersaturation in a solution after the removal of precipitated solids. Though it is an inexact approximation of the true unit of measure, turbidity is used as the primary, real time method of evaluating the effectiveness of a given set of parameters. Turbidity is a measure of light scattering through a solution. Several characteristics of the system, including the size and density of particles in solution, as well as the optical properties of the particles, impact the measured turbidity, making it an approximation, and not a direct measure, of the amount of solids suspended in solution. Furthermore, measuring turbidity

from the outflow does not account for any solids that have scaled along the surface of the pipe or static mixer inserts, or any solids that have settled along the static mixer that are not carried out by the flow. Despite these challenges, turbidity was selected for this initial investigation due to timely data availability and economy considerations.

At the conclusion of the trial, the feed tubes are removed from the solutions, placed in an empty bucket, and the pumps are opened to allow the solution in the mixer to drain. An acid solution is prepared using 6 L DI water and around 160 mL of hydrochloric acid, HCl. The pump tubing is then changed from the MasterFlex 0.03” diameter tubing to the MasterFlex 0.31” diameter tubing, with the MasterFlex 0.03” diameter tubing then cleaned using a DI water squirt bottle. The used cuvettes are placed in the acid solution, as well as the pump leads, and the pump is run at 40 RPM until the acid solution is finished, around 20 min. The bucket and cuvettes are then rinsed with tap water, the cuvettes are set aside to dry, and the bucket is filled with around 1 L of tap water. The tap water is then pumped through the mixer until the outflow conductivity measures  $< 130 \mu\text{S}$ . The bucket is then emptied and filled with around 1 L of DI water, and the pump is run until the outflow measures  $< 20 \mu\text{S}$ . The mixer is then emptied and disassembled. If there are no further trials for the day, the tubs are dumped and washed thoroughly with DI water and set aside to dry. This experimental procedure will be referred to as “procedure 1”. If some portion of this procedure does not have any changes to it explicitly mentioned and defined while a new procedure is detailed, then it can be assumed that portion is unchanged from above. For example, the cleaning procedure never changes throughout the course of this thesis, while more than five different solution compositions were used.

## **2.2 Determining Viable Model Solution**

The purpose of this section is to detail the changes and the rationale for these changes to the previously detailed experimental procedure. For this reason, though experimental results and analysis and discussion of these data will be covered in the following chapter, some results and discussion are necessary in this section to properly explain choices made.

The first set of experiments were conducted to determine the relationship between pump RPMs and associated flow rates and residence time, become familiar with the intricacies of the peristaltic pump, determine methods for ensuring consistent and equal flow rates for both solutions, and generally troubleshoot the experimental apparatus and procedure. One major problem identified with the first set of results that remained an issue through all experiments run was a lack of reproducibility in results. Identifying and eliminating sources of variability between runs of the same set of parameters was a major priority throughout the project. Due to the length of time needed to approach steady state, variability in startup conditions, number of parameters of interest, time necessary to prepare solutions, and the time needed to set up and take apart the apparatus, the number of repetitions at each set of parameters is limited. Therefore, to achieve statistically significant results, it is essential to minimize variability. For this reason, one of the main goals throughout the project was to identify and eliminate sources of variability in the experimental procedure.

The next problem that arose was  $\text{CaCl}_2$  solubility in solution preparation.  $\text{CaCl}_2$  solubility is highly dependent on temperature. For the first several weeks of running these experiments, the ambient temperature outside was high enough that the DI water being used to dissolve the  $\text{CaCl}_2$  had a high enough temperature to fully dissolve the  $\text{CaCl}_2$ . However, as the outside temperature dropped due to the changing seasons, the water being pumped into the lab became colder and colder (the lab deionizing equipment does not adjust the water temperature) until the requisite

CaCl<sub>2</sub> was no longer fully dissolving in 2 L of water. The temperature of water was measured as low as 12° C, down from a temperature of 21° C when the outside temperature was higher. Two solutions to this problem that were investigated were heating the water before dissolving the CaCl<sub>2</sub> and using more water (3 L vs 2 L) to dissolve the CaCl<sub>2</sub>. While both solutions ultimately did lead to fully dissolved CaCl<sub>2</sub>, they complicated the procedure, and, more importantly, introduced the possibility of variability between solutions unless careful attention was given to determining and formalizing a new procedure. Ultimately, the solution that was implemented was to switch from CaCl<sub>2</sub> in the anhydrous form to an equivalent mass of the hydrated form, which significantly increased the solubility of the CaCl<sub>2</sub>. The resulting solution, with the same components as solution 1 shown in table 1, except with an equivalent amount of CaCl<sub>2</sub> dihydrate used instead of CaCl<sub>2</sub> anhydrous, is referred to as solution 2. While changing from the anhydrous to the dihydrate form did impact turbidity, since the molar concentrations of the solutions did not change, solution 2 has the same SI<sub>c</sub> as solution 1 of 764.

After four trials using solution 2, the turbidities of all failed to rise above 5 NTU. Because of the variability in turbidity measurements, which can be affected by factors such as air bubbles in solution and non-uniform crystal densities, as well as the inherent variability in the instruments readings, the statistical certainty in results is increased with increasing turbidity, as the signal to noise ratio in the turbidity readings rises. For this reason, solution 2 produces turbidities too low for the results to be useful. To increase the resulting turbidity from a solution across all sets of parameters, and therefore the amount of calcite that precipitates, it is necessary to increase the degree of supersaturation. Since the precipitation of calcite is governed by equation 4, the degree of supersaturation can be increased by increasing the concentration of either Ca<sub>2</sub><sup>+</sup> ions or CO<sub>3</sub><sup>2-</sup>

ions. To achieve this, the amount of  $\text{CaCl}_2$  and  $\text{NaHCO}_3$  added were both increased by 50%. The resulting inputs for the constituent solutions are shown in table 2.

**Table 2:** Chemical inputs for the two constituent solutions of solution 3.

Constituent	Solution 3A	Solution 3B
$\text{H}_2\text{O}$ (L)	0.5	0.5
$\text{CaCl}_2$ (dihydrate) (g)	3.8840	0
$\text{MgSO}_4$ (heptahydrate) (g)	1.2264	0
$\text{Na}_2\text{SO}_4$ (g)	0	1.5624
$\text{NaHCO}_3$ (g)	0	2.3436

Solution 3 resulted in a  $\text{SI}_c$  of 1932. A 50% increase in amount added for those two salts was determined to be a reasonable starting point. While the resulting turbidities need to be higher than solution 2 to be useful, the lowest degree of supersaturation needed to achieve useful turbidities is the target, as this is the best model for real brine solutions. Additionally, a lower supersaturation results in a lower cost needed to produce the solution, makes it easier to clean the experimental apparatus, and minimizes deposition of solids in the mixer.

To increase the degree of supersaturation from solution 2, the ratios of ions established from the original Brighton, Co based solution needs to be changed, as increasing the supersaturation with this ratio results in supersaturation being achieved in the constituent solutions before they are mixed. In other words, crystals begin to form before the solutions are mixed together. This supersaturation is noted due to crystals visibly forming and theoretically confirmed by OLI Stream Analyzer® software. Therefore, a solution needed to be produced that had a different

ratio of salts added such that no precipitation forms in the two constituent solutions, while maintaining a higher level of supersaturation than solution 3. To achieve this, the relative level of  $\text{MgSO}_4$  is decreased. Using OLI software to ensure no supersaturation is reached in the two component solutions, a solution that matches those two criteria was formulated. The components of this new solution, known as solution 4, is shown in table 3.

**Table 3:** Chemical inputs for the two constituent solutions of solution 4.

Constituent	Solution 4A	Solution 4B
$\text{H}_2\text{O}$ (L)	0.5	0.5
$\text{CaCl}_2$ (dihydrate) (g)	5.9938	0
$\text{MgSO}_4$ (heptahydrate) (g)	0.9008	0
$\text{Na}_2\text{SO}_4$ (g)	0	3.6166
$\text{NaHCO}_3$ (g)	0	3.6166

This solution results in a  $\text{SI}_c$  of 2940. One important distinction between this solution and previous solutions is that in addition to being supersaturated for calcite, this solution is supersaturated for gypsum and has a  $\text{SI}_g$  of 2.12.

Finally, after once more increasing the amount of salts added, solution 5 was formulated, with the inputs shown in table 4. This solution had a high enough supersaturation to ensure results in a useful range and was used for all subsequent experiments until otherwise noted, and has a  $\text{SI}_c$  of 4067 and  $\text{SI}_g$  of 3.585.

**Table 4:** Chemical inputs for the two constituent solutions of solution 5.

Constituent	Solution 5A	Solution 5B
H <sub>2</sub> O (L)	0.5	0.5
CaCl <sub>2</sub> (dihydrate) (g)	7.4917	0
MgSO <sub>4</sub> (heptahydrate) (g)	0.9991	0
Na <sub>2</sub> SO <sub>4</sub> (g)	0	4.5208
NaHCO <sub>3</sub> (g)	0	4.5208

### 2.3 Improving Sampling Procedure

As mentioned in section 2.1, turbidity is an inexpensive and fast measurement, but it is only an estimation of the degree of supersaturation, the true figure-of-merit. To address this, inductively coupled plasma mass spectrometry (ICP-MS), analysis is needed. ICP-MS analysis, which measures the concentration of a dissolved ion, in this case Ca<sup>2+</sup>, is used to conduct a mass balance and accurately measure the difference between the Ca<sup>2+</sup> concentration in the feed solution, and the outflow solution after it has been filtered to remove all solids. Based on this mass balance, any difference between these measurements indicates a corresponding amount of calcite precipitation. This data can then be used to calculate degree of depletion achieved.

As a result of introducing this analysis, both the experimental apparatus and the sampling procedure are altered. To begin, instead of turbidity, conductivity, and pressure drop measurements being taken every five min, they are taken every ten min. Additionally, instead of finishing an experiment if measured turbidities were consistently low at 30 min, all experiments

were continued until 90 min from the leading edge of the solution reaching the outflow. Another change was the introduction of taking a sample of solution from the second inflow T-junction, after the solutions had mixed but before entering the static mixer. To allow these samples to be taken, an additional T-junction was added to the apparatus where the pressure monitor's tubing had previously been attached. A side-by-side comparison of the old and new apparatus set ups is shown in figure 12.



**Figure 12:** Side by side comparison of old (left) and new (right) experimental apparatus setups. The inflow samples were taken at 20, 40, 60 and 80 min by injecting a long needle through the septum at the top of the new, additional T-junction piece and drawing a 10 mL sample with a syringe. That sample is then moved to a marked collection tube and mixed with 0.11 mL 69 w% Fisher Chemical nitric acid,  $\text{HNO}_3$  to dissolve any precipitation and prevent any new precipitation from occurring. In addition to taking these inflow measurements, written observations are also taken at 20, 40, 60 and 80 min. Finally, at 30, 60, and 90 min, a sample is taken from the outflow. This sample is taken by placing a beaker under the outflow for 3 min,

swirling to prevent any precipitation from settling, then drawing 20 mL of solution with a syringe. This sample is then pushed through a membrane held in a 25 mm Cole-Parmer membrane filter holder, into a marked collection tube, and 0.22 mL HNO<sub>3</sub> is added. The membranes used are Donaldson Tetratex 50 nm PTFE membranes cut to size, marked and weighed. A schematic of this sampling procedure is shown in figure 13.

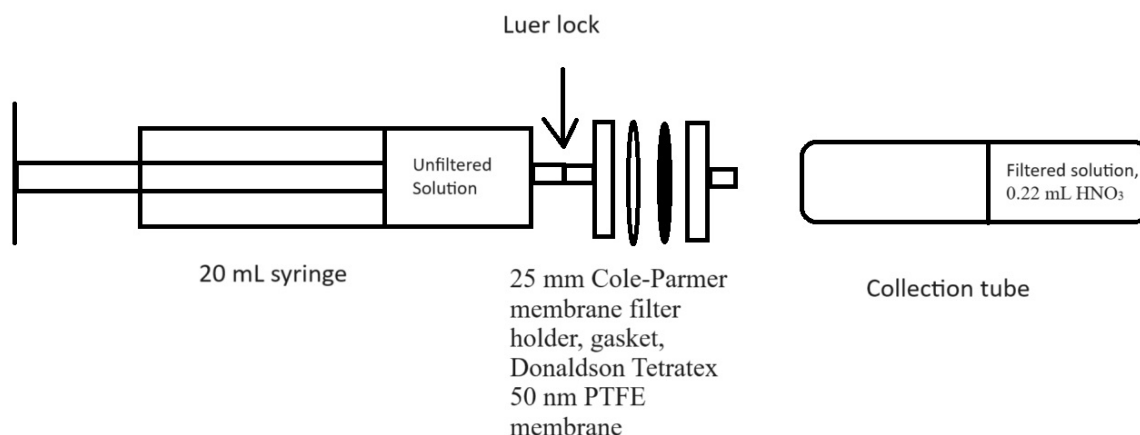


**Figure 13:** Schematic of sample filtration apparatus.

Five membranes are cut and labeled for each experiment. Membrane 1 goes directly into an oven at 50 C, membrane 2 is wetted with ethanol then placed in the oven, while membranes 3-5 are prewetted with ethanol, used to filter the 20 mL samples, then also placed in the oven. The membranes are dried for 12-36 h, then weighed once more. This new procedure will be referred to as “procedure 2”. A summary of sampling procedures used in this project is provided in appendix A.

After formulating this new procedure, the effect on resulting turbidities of the changed inflow apparatus set up is investigated. Experiments are run with five different sets of parameters both with and without the added T-junction, with the results summarized in table 5.

**Table 5:** Summary of experiments run at 48” length, 0.5” diameter, and solution 5 for both the inflow apparatus constructed with two T-junctions (old) and three T-junctions (new) with the same sets of parameters.

			Old inflow	Old inflow	Old inflow	New inflow	New inflow	New inflow
Shape	Material	approximate observed residence time (min)	turbidity, t = 30 min, NTU	turbidity, t = 60 min, NTU	turbidity, t = 90 min, NTU	turbidity, t = 30 min, NTU	turbidity, t = 60 min, NTU	turbidity, t = 90 min, NTU
Shell	PETG	7	16.2	10.2	5.85	22.2	7.65	1.28
Farfalle	PETG	7	26.4	7.12	4.76	13	19.5	4.3
Shell	PC	7	4.25	4.87	4.08	2.18	0.75	1.72
Rotelle	PETG	7	0.95	0.5	0.51	1.85	0.54	0.59
Hourglass	PETG	7	30.5	20.8	14.5	51.4	34.7	16.4

The results of a 2-sample Kolmogorov-Smirnov test, shown in figure 14, indicate no statistical difference in the results from the two setups at 90 min. The use and limitations of this statistical test is discussed in the data analysis section. Though the results would be more rigorous with more than 5 paired data points, with four degrees of freedom and an alpha value of 0.87, additional data points are very unlikely to change the statistical outcome.

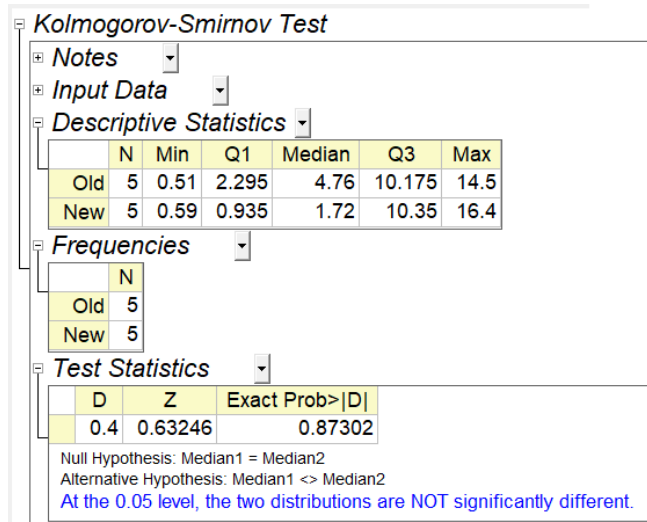


**Figure 14:** Results of a 2-sample Kolmogorov-Smirnov tests examining resulting turbidities at 90 min for five distinct sets of parameters for both experimental apparatus', using two and three inflow T-junctions.

After determining that there is likely no significant difference between the two apparatus setups in the resulting turbidites, the diameter of the pipe used is changed from 0.5” to 1”. This change is in part an attempt to reduce variability within runs of the same sets of parameters. One consequence of this change is an increase in the flow rates necessary to achieve the selected residence times, and subsequently an increase in the total volume of solution needed to run an experiment for 90 min. This led to the discovery that the solutions were not reaching equilibrium with atmospheric CO<sub>2</sub> in the time frame being used. This disequilibrium means that the exact composition of the solution was variable and unknown. This issue, and the response to it are discussed in appendix B. However, in the time period between the discovery of this issue and the formulation of a solution, which ended up changing both solution compositions and the procedure for solution preparation, many experiments were run using solution 5.

The components of the new solution devised in Appendix B to solve the atmospheric disequilibrium issue are shown in table 6.

**Table 6:** Chemical inputs for the two constituent solutions of solution 6.

Constituent	Solution 6A	Solution 6B
H <sub>2</sub> O (L)	0.5	0.5
CaCl <sub>2</sub> (dh) (g)	3.087	0
MgSO <sub>4</sub> (heptahydrate) (g)	0	3.053
Na <sub>2</sub> SO <sub>4</sub> (g)	0.2758	0
NaHCO <sub>3</sub> (g)	0	1.368
NaOH (g)	0.075	0

Solution 6 results in a  $SI_c$  of 5399. This solution is prepared with the same procedure as previous solutions, with four changes. First, when dissolving all salts, care is taken to remove the beaker from the stir plate and add the solution to the tubs in as little time as possible while still ensuring the salts fully dissolve. Second, VWR Chemicals NaOH 50% w/w is added to solution 6a after the solution is otherwise fully prepared whilst stirring the solution. Third, as soon as solutions are fully prepared, they are capped, remain capped throughout the procedure, and experiments are run immediately after preparation to limit gas exchange. Finally, the same amount of solution, 12 L, is produced every time, regardless of necessary flow rates, and a fresh solution is prepared for each experiment, even if they occur on the same day. A summary of the differences between all the used solutions is shown in table 7.

**Table 7:** Table showing saturation index and which salt species are supersaturated for the six solutions used in this work.

solution #	SI <sub>c</sub>	salt species supersaturated
1	764	Calcite
2	764	Calcite
3	1932	Calcite
4	2940	Calcite, Gypsum
5	4067	Calcite, Gypsum
6	5399	Calcite

The first round of results from ICP-MS analysis showed that sampling the solution through the new inflow T-Junction shown in figure 12 did not result in a good estimation of the Ca<sup>2+</sup> concentration before crystallization occurs due to the solutions not being thoroughly mixed where the sampling takes place. This instigated the final change to the experimental procedure, removing the new inflow T-junction and returning to original inflow setup. To replace this sample as a measure of the calcium concentration of the fully supersaturated solution, a sample is taken directly from constituent solution with the dissolved CaCl<sub>2</sub> before the experiment is begun. Furthermore, the outflow sample that is filtered is increased from 20 mL to 100 mL, and the membrane is housed in a 47 mm Sartorius In-Line Stainless Steel Filter Holder. This procedure is referred to as “procedure 3”. A summary of sample procedures is shown in Appendix A.

## Chapter 3

### 3.1 Raw Experimental Results

The raw results for all experiments following procedure 1 (no solids filtration or sampling) are shown in table 8. The experimental results for all experiments following procedure 2 (inflow and outflow sampling) and procedure 3 (outflow sampling, direct solution sampling, and increased filtration volume) are shown in table 9.

**Table 8:** Experimental results for all experiments run using procedure 1.

shape	material	targeted Tau (min)	flow rate (mL/sec)	tubing length (in)	solution	Tubing diameter (in)	Turbidity (NTU)										procedure	Kolmogorov mixing length (m)
							10 min	20 min	30 min	40 min	50 min	60 min	70 min	80 min	90 min			
Farfalle	PETG	3	0.726	48	1	0.5	7.64	7.45	6.22	6.86	6.74	6.88	0	0	0	1	0.0001031	
Hourglass	PETG	3	0.473	48	1	0.5	8.05	7.86	7.1	7.11	5.87	6.11	5.48	0	0	1	9.6664E-05	
Rotelle	PETG	3	0.306	48	1	0.5	10.3	8.32	7.01	6.52	6.15	5.9	5.6	0	0	1	0.00011082	
Shell	PETG	3	0.707	48	1	0.5	8.12	8.11	7.38	6.78	6.74	6.19	6.18	5.79	5.72	1	0.00010011	
Farfalle	PETG	7	0.300	48	1	0.5	6.75	6.3	6.44	6.51	6.08	6.26	0	0	0	1	0.00013265	
Hourglass	PETG	7	0.191	48	1	0.5	4.43	4.02	3.72	3.28	3.12	2.84	0	0	0	1	0.00013253	
Rotelle	PETG	7	0.197	48	1	0.5	12.7	9.86	7.56	6.07	5.17	4.74	4.61	4.57	3.96	1	0.00012743	
Shell	PETG	7	0.281	48	1	0.5	23.3	19.5	16.5	16.3	14.6	13.7	13.9	13.1	12.9	1	0.00013212	
Farfalle	PETG	11	0.203	48	1	0.5	16.6	17.1	17.2	16.4	15.7	14.7	14.7	14.3	13.3	1	0.00014999	
Hourglass	PETG	11	0.129	48	1	0.5	12.4	9.32	8.66	7.33	6.89	6.58	6.84	6.11	0	1	0.00014816	
Rotelle	PETG	11	0.114	48	1	0.5	14.6	12.7	8.79	7.7	6.76	6.09	5.32	5.06	4.63	1	0.00014598	
Shell	PETG	11	0.183	48	1	0.5	24.8	20.9	17.8	16.5	15.9	13.4	12.9	13.1	0	1	0.00014657	
Rotelle	PETG	3	0.306	48	2	0.5	2.68	0.62	0.41	0	0	0	0	0	0	1	0.00011082	
Farfalle	PETG	7	0.300	48	2	0.5	0.65	0	0	0	0	0	0	0	0	1	0.00013265	
Shell	PETG	7	0.281	48	2	0.5	3.59	0	0	0	0	0	0	0	0	1	0.00013212	
Shell	PETG	7	0.281	48	2	0.5	34.2	15.8	7.07	3.89	2.29	1.76	0	0	0	1	0.00013212	
Shell	PETG	7	0.281	48	2	0.5	0.55	0.7	0	0	0	0	0	0	0	1	0.00013212	
Shell	PETG	7	0.281	48	2	0.5	0.35	0	0	0	0	0	0	0	0	1	0.00013212	
Shell	PETG	7	0.281	48	2	0.5	0.38	0	0	0	0	0	0	0	0	1	0.00013212	
Shell	PETG	7	0.281	48	2	0.5	1.33	2.05	2.53	2.01	1.89	1.73	0	0	0	1	0.00013212	
Shell	PETG	7	0.281	48	2	0.5	0.38	0.32	0.34	0	0	0	0	0	0	1	0.00013212	
Farfalle	PETG	11	0.203	48	2	0.5	0.39	0	0	0	0	0	0	0	0	1	0.00014999	
Hourglass	PETG	11	0.129	48	2	0.5	0.35	0	0	0	0	0	0	0	0	1	0.00014816	
Shell	PETG	11	0.183	48	2	0.5	0.68	0.34	0.33	0	0	0	0	0	0	1	0.00014657	
Farfalle	PETG	3	0.726	48	3	0.5	0.43	0.51	0.34	0	0	0	0	0	0	1	0.0001031	
Hourglass	PETG	3	0.473	48	3	0.5	1.51	0.42	0.57	0.43	0	0	0	0	0	1	9.6664E-05	
Shell	PETG	3	0.707	48	3	0.5	0.48	0.45	0.33	0	0	0	0	0	0	1	0.00010011	
Hourglass	PETG	7	0.191	48	3	0.5	3.08	4.08	3.44	2.43	2.33	2.09	0	0	0	1	0.00013253	
Rotelle	PETG	7	0.197	48	3	0.5	0.57	0.5	0.62	0	0	0	0	0	0	1	0.00012743	
Shell	PETG	7	0.281	48	3	0.5	0.59	12	18.2	20.2	19.7	17.5	12	10.3	7.98	1	0.00013212	
Shell	PETG	7	0.281	48	3	0.5	3.67	2.39	2.15	1.83	1.5	1.28	0	0	0	1	0.00013212	
Shell	PETG	7	0.281	48	3	0.5	14.9	7.48	4.98	3.25	1.95	1.42	0	0	0	1	0.00013212	
Rotelle	PETG	7	0.197	48	4	0.5	7.78	4.12	5.2	3.75	2.93	2.76	0	0	0	1	0.00012743	
Shell	PETG	7	0.281	48	4	0.5	7.52	6.55	5.87	5.72	5.72	5.41	5.64	5.25	5.44	1	0.00013212	
Farfalle	PETG	3	0.726	48	5	0.5	12.6	9.44	9.06	9.28	8.38	8.61	0	0	0	1	0.0001031	
Farfalle	PETG	3	0.726	48	5	0.5	136	109	97.5	42.9	41.3	38.4	0	0	0	1	0.0001031	
Farfalle	PETG	3	0.726	48	5	0.5	53.4	32.2	23.1	20.1	18.8	17.6	18.5	20.5	0	1	0.0001031	
Hourglass	PETG	3	0.473	48	5	0.5	129	133	71.4	54.6	44.9	36.2	0	0	0	1	9.6664E-05	
Hourglass	PETG	3	0.473	48	5	0.5	22.7	8.47	7.59	6.86	6.48	6.83	0	0	0	1	9.6664E-05	
Hourglass	PETG	3	0.473	48	5	0.5	31.5	18	14.6	13.3	11.6	10.3	0	0	0	1	9.6664E-05	
Hourglass	PETG	3	0.473	48	5	0.5	49.8	33.8	17.9	11.2	8.15	0	0	0	0	1	9.6664E-05	
Rotelle	PETG	3	0.306	48	5	0.5	21.5	15	10.3	6.59	7.32	9.88	0	0	0	1	0.00011082	
Rotelle	PETG	3	0.306	48	5	0.5	62	39.5	23.6	11.9	6.03	4.47	0	0	0	1	0.00011082	
Shell	PETG	3	0.707	48	5	0.5	296	250	197	156	99.3	69.3	60.9	57.1	0	1	0.00010011	
Shell	PETG	3	0.707	48	5	0.5	1.47	6.31	8.93	10.3	10.2	9.34	0	0	0	1	0.00010011	
Shell	PETG	3	0.707	48	5	0.5	2.72	4.47	6.99	7.77	0	0	0	0	0	1	0.00010011	
Farfalle	PETG	7	0.300	48	5	0.5	32.9	34.9	30.4	25.7	31.4	26.5	26.1	23.2	24	1	0.00013265	
Farfalle	PETG	7	0.300	48	5	0.5	24	23.4	20.1	19.6	17.7	21.8	0	0	0	1	0.00013265	
Hourglass	PETG	7	0.191	48	5	0.5	16.9	14.5	12.8	10.1	7.81	6.85	0	0	0	1	0.00013253	
Rotelle	PETG	7	0.197	48	5	0.5	20.1	9.32	7.81	5.43	5.16	5.59	0	0	0	1	0.00012743	
Shell	PETG	7	0.281	48	5	0.5	23.1	16.2	20.7	20	15.2	14.7	13.3	13.1	15.2	1	0.00013212	
Shell	PETG	7	0.281	48	5	0.5	68.3	37.9	19	17.6	16.4	12.7	7.81	0	0	1	0.00013212	
Shell	PETG	7	0.281	48	5	0.5	23.5	20.9	20	17.3	19.1	18.2	13.2	23.3	16.2	1	0.00013212	
Shell	PETG	7	0.281	48	5	0.5	54	37.3	20.8	19.5	12.6	13.8	0	0	0	1	0.00013212	
Shell	PETG	7	0.281	48	5	0.5	53.4	21.5	22.8	21.5	17	15.4	0	0	0	1	0.00013212	
Shell	PETG	7	0.281	48	5	0.5	31.1	18	12.5	14.9	12.1	14.5	0	0	0	1	0.00013212	
Shell	PETG	7	0.281	48	5	0.5	30	16.5	10.7	5.1	2.45	2.34	0	0	0	1	0.00013212	
Shell	PETG	7	0.281	48	5	0.5	39	22.9	17	13.9	8.91	9.26	0	0	0	1	0.00013212	
Shell	PETG	7	0.281	48	5	0.5	4.91	5.15	4.86	2.91	3.67	4.67	0	0	0	1	0.00013212	
Farfalle	PETG	11	0.203	48	5	0.5	10.6	4.26	4.68	4.2	0	0	0	0	0	1	0.00014999	
Hourglass	PETG	11	0.129	48	5	0.5	25.8	14.7	11.4	12.3	9.62	8.2	9.91	8.8	0	1	0.00014816	
Rotelle	PETG	11	0.114	48	5	0.5	6.12	23.8	6.36	9.61	5.75	4.8	0	0	0	1	0.00014598	
Shell	PETG	11	0.183	48	5	0.5	18.6	11.7	7.73	5.67	5.2	5.88	0	0	0	1	0.00014657	
Shell	PETG	11	0.183	48	5	0.5	8.37	12.7	9.94	10.1	9.54	7.18	0	0	0	1	0.00014657	
Shell	PETG	11	0.183	48	5	0.5	44.4	30.7	23.2	18.8	15.7	16.6	0	0	0	1	0.00014657	
Farfalle	PETG	6	0.699	96	5	0.5	52.8	35.4	28.5	18.8	6.37	1.32	0	0	0	1	0.00010067	
Farfalle	PETG	6	0.699	96	5	0.5	72.2	38.1	24.1	17	13.5	8.29	5.46	0	0	1	0.00010067	
Farfalle	PETG	6	0.699	96	5	0.5	150	99.7	74.2	63.5	47.6	43.1	0	0	0	1	0.00010067	
Farfalle	PETG	6	0.699	96	5	0.5	2.89	2.7	2.15	2.17	2.55	0	0	0	0	1	0.00010067	
Farfalle	PETG	6	0.699	96	5	0.5	2.41	1.87	1.93	3.91	0	0	0	0	0	1	0.00010067	
Hourglass	PETG	6	0.567	96	5	0.5	25.6	2.76	1.79	2.14	0	0	0	0	0	1	9.1723E-05	
Rotelle	PETG	6	0.380	96	5	0.5	19.7	2.61	2.33	2.2	0	0	0	0	0	1	0.00010237	
Shell	PETG	6	0.711	96	5	0.5	17.9	18.3	14.6	12.7	12.3	11.8	0	0	0	1	9.7324E-05	
Shell	PETG	6	0.711	96	5	0.5	2.81	2.87	2.49	3.31	0	0	0	0	0	1	9.7324E-05	
Farfalle	PETG	14	0.301	96	5	0.5	2.77	2.49	1.02	1.44	0	0	0	0	0	1	0.00012405	
Farfalle	PETG	14	0.301	96	5	0.5	22.8	1.69	6.26	7.48	5.96	5.22	0	0	0	1	0.00012405	
Farfalle	PETG	14	0.301	96	5	0.5	9.66	1.23	1.42	1.62	0	0	0	0	0	1	0.00012405	
Hourglass	PETG	14	0.223	96	5	0.5	92	12.6	8.57	2.11	6.59	6.01	0	0	0	1	0.0001192	
Rotelle	PETG	14	0.200	96	5	0.5	0.84	0.43	0.61	0	0	0	0	0	0	1	0.00011882	
Rotelle	PETG	14	0.200	96	5	0.5	2.5	1.07	1.67	0	0	0	0	0	0	1	0.00011882	
Rotelle	PETG	14	0.200	96	5	0.5	3.05	2.23	1.85	0	0	0	0	0	0	1	0.00011882	
Shell	PETG	14	0.264	96	5	0.5	6.53	2.36	2.16	0	0	0	0	0	0	1	0.00012593	



In table 9, solution 7 refers to solutions prepared using the same components at solution 5, but at larger sizes than 6 L such that the composition and saturation index are distinct.

### **3.2 Data Analysis**

One of the major takeaways from this data is the variability and lack of reproducibility amongst results from experiments run with the same set of parameters. This variability decreases the strength of any statistical analysis, and the reason many of these experiments were run was to attempt to isolate and determine factors causing variability. One such factor that was examined thoroughly was the exact conditions when initially starting an experiment, such as bubbles in the feed lines, which solution reached the inflow T-junction first, and what pump RPM was used to fill the feed lines. While the focus on particular parts of the procedure probably did eventually slightly lower the variability, the main factors causing variability were likely the different exact compositions of the solutions at the time of their use due to varying amounts of time between initial preparation and the start of the experiment, an issue that is discussed in Appendix B, and variability due to variation in exact mixing patterns and other factors inherent in the experimental protocols. All statistical tests and plots are done in OriginPro 2023 (Academic) software or using the “statsmodels” open-source Python module.

To begin analysis, the effectiveness of turbidity as a measure of depletion is investigated. A plot of the depletion achieved from experiments run using solution 5, procedure 2, with a 1” diameter and a length of 48”, and turbidity is shown in figure 15. This data has had outlier values omitted, with an outlier being defined as a point separated from either of the other two values by more than twice the difference between these other two values.

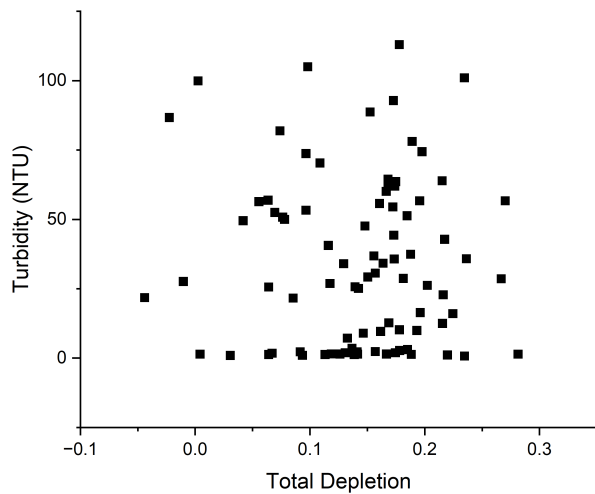
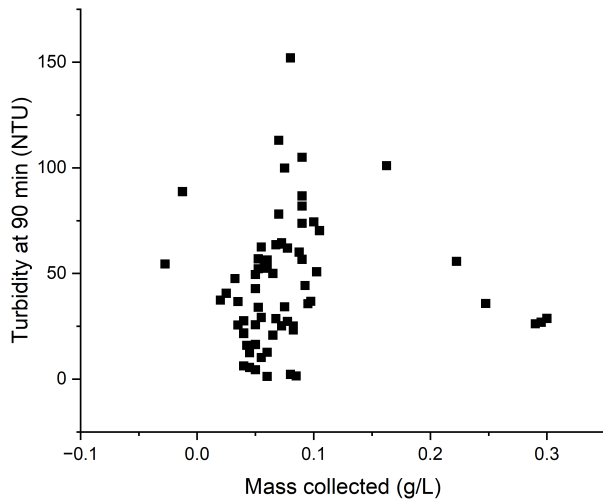


**Figure 15:** A plot of total depletion and turbidity for experiments at 1" diameter, 48" length and solution 5.

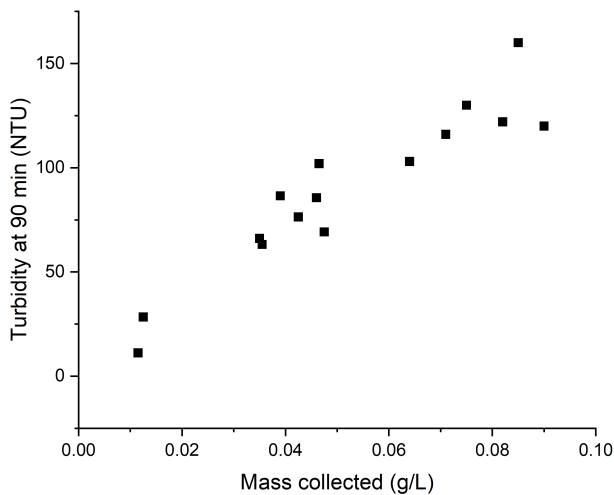
This plot shows no clear relationship between turbidity and depletion. There are several factors that might account for the lack of any trend. A previously mentioned factor is that turbidity measurements are only an estimation of crystal density in a solution, with factors such as chemical composition, morphology and size of the crystals impacting the turbidity readings. Another factor driving this is solids forming in the mixer that do not make it to the outflow, either through deposition, scaling, or some other process. These solids will be accounted for in ICP-MS analysis, but not turbidity readings. These two factors are the main reasons that ICP-MS analysis is employed, as theoretically ICP-MS analysis provides a true measure of depletion and therefore precipitation formed, instead of the estimation provided by turbidity readings. However, based on this data, it seems likely that there are issues with the ICP-MS values that are more severe than the two previously mentioned issues with turbidity readings, preventing a clear relationship between the two sets of values. The first major issue is that when filtering out solids, and therefore creating the filtered samples for ICP-MS analysis, there were multiple instances of

leaking from the membrane holder. This leaking produced sample that did not get filtered, as the leaks were caused by high pressure exerted on unfiltered sample to pass it through the membrane. It is possible that some of this unfiltered sample leaked out of the membrane holder and ended up in the collection tube with the filtered sample, resulting in an ICP-MS value with a higher calcium concentration than the true solution value (this results in a lower estimated depletion than actually occurred). The second major issue is problems with conducting the dilutions needed to lower the calcium concentrations of samples to a level that the ICP-MS instrumentation can handle. Though care was taken to make these dilutions as precise as possible, with micropipettes being tested to ensure calibration and ensuring a new pipette tip for every sample, most of the samples were diluted by a factor of 100, so any small errors or variability in the dilution have large impacts in the resulting depletion values. Some combination of these issues has prevented the measured values for both depletion and turbidity from showing the positive correlation that should theoretically be seen. Of these two sets of values, the difficulties with depletion seem more severe than the difficulties with turbidity. As a result, for this work, turbidity will be used as the estimate for induced precipitation. All conclusions made using turbidity values therefore must take into account the imperfect nature of this estimation.

Next, the relationship between turbidity and solids collected is examined. A plot of turbidity and solids collected for experiments run with 1" diameter, 48" length, solution 5 and procedure 2 is shown in figure 16. A plot of turbidity and solids collected for experiments run with 1" diameter, 48" length, solution 6 and procedure 3 is shown in figure 17.



**Figure 16:** A plot of solids collected and turbidity for experiments at 1" diameter, 48" length, solution 5 and procedure 2.



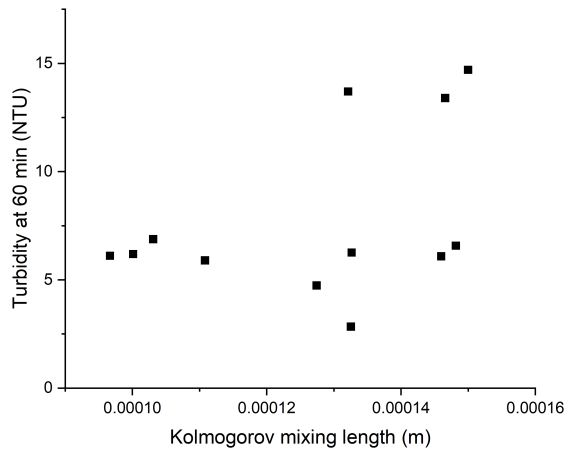
**Figure 17:** A plot of solids collected and turbidity for experiments at 1" diameter, 48" length, solution 6 and procedure 3.

Figure 16 shows no relationship between mass collected and turbidity. This is likely due to challenges with the sampling procedure, as the volume of solution filtered, and solid concentrations are so low that small fluctuations in the scale used to weigh the membranes drastically change the resulting values for the solids collected. Furthermore, the membrane

holder used in procedure 2 was prone to leaking, resulting in portions of the solution included in the volume of solution filtered not actually being filtered, as previously mentioned. Despite the low number of data points, the changes made for procedure 3, including a higher volume of solution filtered, a different membrane holder, a larger membrane and a new scale resulted in a clear linear correlation between solids collected and turbidity. This result shows that although turbidity and mass collected do not account for solids deposited in the static mixer or scaling along the surface of the static mixer, turbidity is a reasonable measure of total solids suspended in solution and that the effect on turbidity by factors such as crystal size and morphology are secondary effects in the context of these experiments. Though, the strength of conclusions drawn from data using turbidity must be carefully qualified, mainly due the impact of solids formed in the static mixer that are not suspended in the outflow solution, it must be used for most of the data analysis due to the previously mentioned issues with depletion and the fact that most of the data was produced using procedure 2.

To investigate the effect of mixing energies, and therefore Kolmogorov mixing lengths, first the turbidity readings at 60 min are averaged for each combination shape, residence time, tube length and solution used for data produced at 0.5" diameter, as well as the turbidity readings at 90 min for 1" diameter. Only data produced using PETG inserts are included due to non-comprehensive data being produced using the other materials. These averaged turbidities are then plotted against Kolmogorov mixing length, shown in figures 18-21.

Data points with no error bars indicate that only one turbidity value exists for that set of parameters.



**Figure 18:** Average turbidities at 60 min for each set of parameters with data at 0.5" diameter, PETG, 48" length and solution 1 plotted against Kolmogorov mixing length.

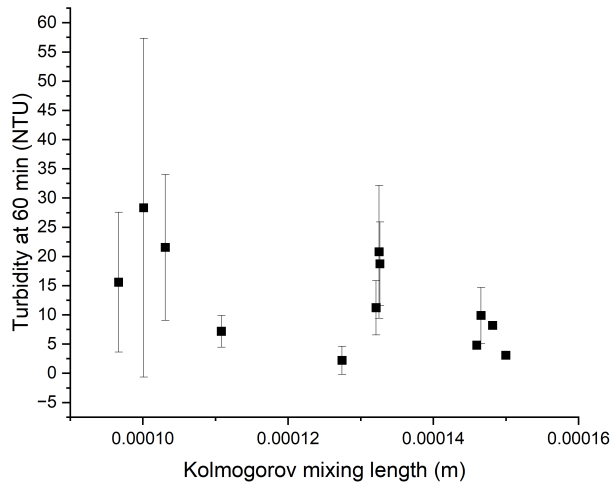


**Figure 19:** Average turbidities at 60 min for each set of parameters with data at 0.5" diameter, PETG, 48" length and solution 5 plotted against Kolmogorov mixing length.

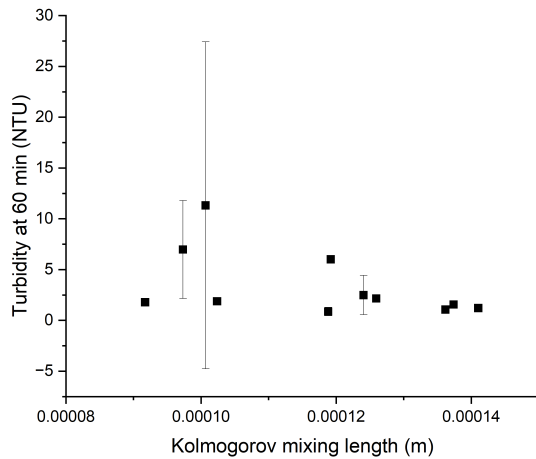


**Figure 20:** Average turbidities at 60 min for each set of parameters with data at 0.5" diameter, PETG, 96" length and solution 5 plotted against Kolmogorov mixing length.

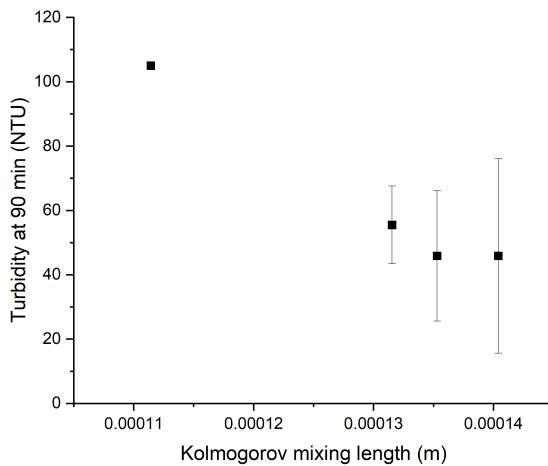


**Figure 21:** Average turbidities at 90 min for each set of parameters with data at 1" diameter, PETG, 48" length and solution 5 plotted against Kolmogorov mixing length.

These plots show no clear trends in the relationship between turbidity and mixing lengths, either separately or combined. In previous work by the group, investigating rates of precipitation of calcite using a CSTRs-in-series apparatus found a strong correlation between precipitation rate and the combination of mixing energy, and therefore power dissipation and Kolmogorov mixing length, and the surface area-to-volume ratio of the mixing region<sup>24</sup>. The same paper showed that

residence time also affects the rate of precipitation in CSTRs-in-series. One reason this data fails to show a relationship between Kolmogorov mixing length and produced turbidity is that for a CSTRs-in-series apparatus, mixing length can be varied independently without affecting residence time or flow rate. For the static mixer apparatus in this work, mixing length is varied by changing the flow rate of solution, meaning the mixing length cannot be altered without also changing the flow rate and residence times. This inability to independently change the mixing length makes establishing a relationship between turbidity and mixing length less straightforward than when using CSTRs-in-series. Furthermore, the surface area to volume ratio varies across the different shapes of inserts used further complicating the picture. Attempts to limit both these effects by segregating data points by residence time, with the resulting plots shown in Appendix C, again fail to show any clear correlation or relationship between mixing length and turbidity.

Finally, and perhaps most crucially, in this work mixing length is calculated using a pressure drop value across the entire static mixer apparatus and is therefore an average of mixing lengths across the static mixer. In a CSTRs-in-series apparatus, an average mixing length can be informative of the fluid dynamic conditions of a relatively homogeneous mixer. In contrast, a static mixer apparatus produces relatively heterogeneous fluid dynamic conditions across the mixer. An averaged mixing length therefore does not properly quantify or explain the unique set of localized fluid dynamic conditions for each combination of flow rate, insert shape used, and length and diameter of tubing. Further work is needed to separate the effects of the combination of the three factors mentioned, and it may prove that a different metric than mixing length is more useful in elucidating a generalized relationship between mixing conditions and precipitation in static mixers.

Next, the effect of shape, material and residence time on turbidity is investigated. Averaged turbidities at 60 min are plotted against shape and residence times for PETG and 48" length, with solution 1 and 0.5" diameter shown in figure 22, solution 5 and 0.5" diameter shown in figure 23. Once again, no error bars indicate only one observation.

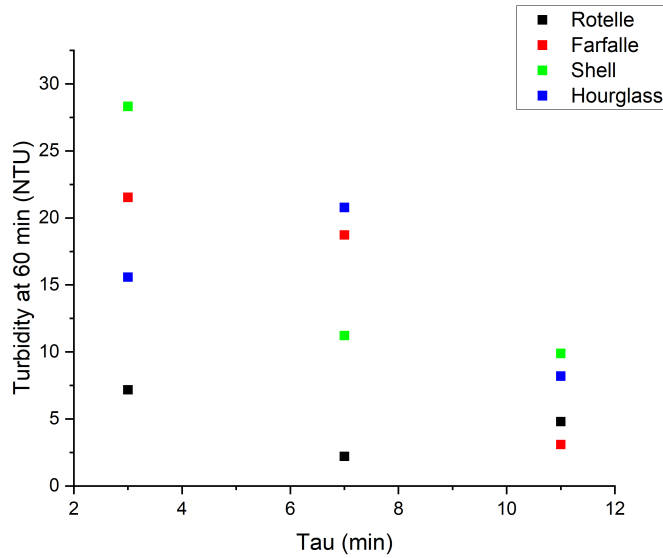


**Figure 22:** Turbidities at 60 min plotted against shape and residence times for PETG, 48" length, solution 1 and 0.5" diameter.

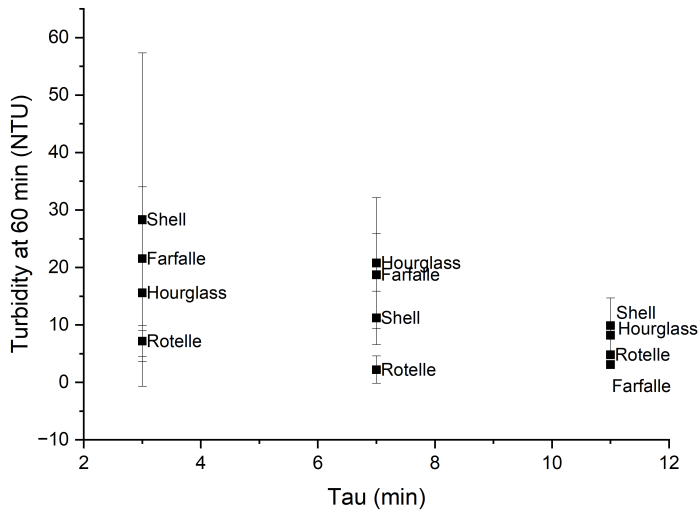


**Figure 23:** Average turbidities at 60 min plotted against shape and residence times for PETG, 48" length, solution 5 and 0.5" diameter.

Figures 22 and 23 seem to show a trend of higher turbidities at lower residence times. This may indicate that for the set of conditions that these plots show, PETG, 48" length and 0.5" diameter, the previously shown effect of higher mixing energy (or some other effect of higher flow rates) leading to increased precipitation dominates the competing effect of lower residence time leading to lower precipitation<sup>24</sup>. However, further statistical analysis is needed to justify any conclusion drawn regarding the effect of shape or residence time.

A 3-way ANOVA test investigating the effects of shape, residence time, and material on turbidities at 60 min for experiments ran using solution 5, 0.5" diameter, and 48" length is shown in figure 24, while the factors and levels included in this dataset are shown in table 10. There are three assumptions that must be met for the results of an ANOVA analysis or Tukey's test of significance to be considered entirely reliable<sup>56</sup>. While this data is independent, and a returned p-value of 0.090 from a Shapiro-Wilk test suggests the data follows a normal distribution, the assumption of equal variance cannot be verified because there are combinations of levels that

have only one data point. While non-parametric tests without the need to prove these assumptions will be used when applicable, the conclusions drawn from ANOVA analysis or Tukey’s test of significance must be qualified by the failure to prove these assumptions. Additionally, the high degree of variability in the number of observations for a given set of levels, for this data set it ranges from 1 to 10, further limiting the strength of conclusions to be drawn from these methods of statistical analysis.

**Table 10:** Table showing the factors and levels for experiments ran using solution 5, at 0.5” diameter, and 48” length.

Factor	Shape	Material	Residence time (min)
Levels	rotelle	PETG	3
	farfalle	PC	7
	shell		11
	hourglass		

	sum_sq	df	F	PR(>F)
Intercept	3524.826	1	21.92443	6.61E-05
C(Shape, Sum)	481.3019	3	0.9979	0.408284
C(Material, Sum)	3153.601	1	19.61542	0.000132
C(Tau, Sum)	487.4982	2	1.51612	0.237044
C(Shape, Sum):C(Material, Sum)	381.2544	3	0.790468	0.509445
C(Shape, Sum):C(Tau, Sum)	540.2347	6	0.560044	0.758156
C(Material, Sum):C(Tau, Sum)	457.3006	2	1.422206	0.258072
C(Shape, Sum):C(Material, Sum):C(Tau, Sum)	645.1483	6	0.668804	0.675457
Residual	4501.604	28		

**Figure 24:** 3-way ANOVA test examining interactions between shape, material, and residence time on turbidities at 60 min for experiments ran using solution 5, at 0.5” diameter, and 48” length.

For this analysis, no statistically significant interactions between the different factors were observed. The only significant result, at an alpha level of 0.05, which will be used for all subsequent analyses in this work, is the effect on turbidity by material. For solution 5, 0.5”

diameter, and 48” length, experiments were only run using inserts of two materials, PETG and PC, and both the experiments run using PC were conducted using shell and a residence time of 7 min. To compare these two materials, a two-sample Kolmogorov–Smirnov test is used. A two-sample Kolmogorov–Smirnov test, a non-parametric test similar to a two-sample t-test, determines the probability that two sets of values are drawn from the same probability distribution by measuring the differences between the two samples’ cumulative distribution functions<sup>57</sup>. The result of this test conducted using the turbidity at 60 min for both PC and PETG for shell, 7 min residence time, solution 5, 0.5” diameter, and 48” length, is shown in figure 25.

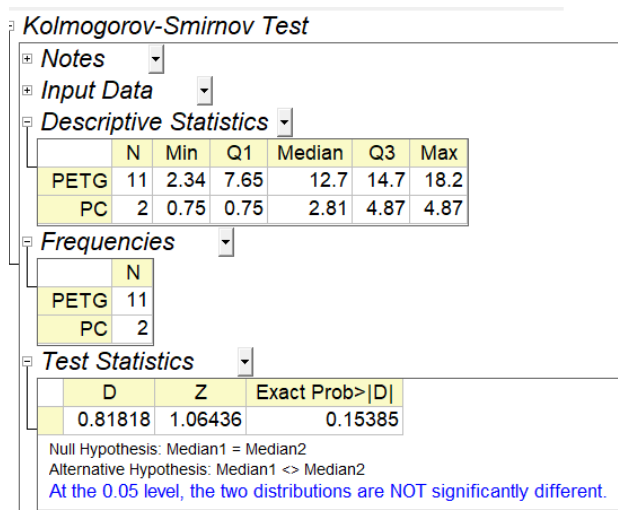


**Figure 25:** Results of two-sample Kolmogorov–Smirnov test comparing turbidities at 60 min for PETG and PC for solution 5, 0.5” diameter, 48” length, 7 min residence time and shell.

In the “Descriptive Statistics” shown in figure 24, “N” refers to the number of observations, “Min” is the minimum turbidity values in the dataset, “Median” is the median turbidity in the dataset, “Max” is the maximum turbidity values in the dataset, and “Q1” and “Q3” refer to the turbidity values corresponding to the 25<sup>th</sup> percentile and 75<sup>th</sup> percentile, respectively. The results of this test show that under the given set of levels, the turbidity at 60 min for PETG and PC is not statistically significant. This is likely due to the low number of experiments conducted using PC.

A two-way ANOVA test examining the effects of shape and residence time on turbidities at 60 min for experiments performed using solution 5, 0.5” diameter, PETG, and 48” length, the same set of levels as the previous test, except only including experiments using PETG, is shown in figure 26, while the factors and levels included in this dataset are shown in table 11.

**Table 11:** Table showing the factors and levels for experiments ran using solution 5, at 0.5” diameter, 48” length, and PETG.

Factor	Shape	Residence time (min)
Levels	rotelle	3
	farfalle	7
	shell	11
	hourglass	

	df	sum_sq	mean_sq	F	PR(>F)
C(Shape, Sum)	3	735.4858	245.1619	1.473225	0.244004
C(Tau, Sum)	2	512.1249	256.0625	1.538728	0.232893
C(Shape, Sum):C(Tau, Sum)	6	658.2184	109.7031	0.659227	0.682744
Residual	27	4493.117	166.4117		

**Figure 26:** 2-way ANOVA test examining interactions between shape and residence time on turbidities at 60 min for experiments ran using solution 5, at 0.5” diameter, 48” length, and PETG.

This test shows no significant impact on turbidity by shape or residence time. This result is expected based on the test shown in figure 24, as only the two non-PETG values were removed to conduct this analysis.

A two-way ANOVA test examining the effects of shape and residence time on turbidities at 60 min for experiments ran using solution 5, 0.5” diameter, PETG, and 96” length, is shown in figure 27, while the factors and levels included in this dataset are shown in table 12.

**Table 12:** Table showing the factors and levels for experiments ran using solution 5, at 0.5” diameter, 96” length, and PETG.

Factor	Shape	Residence time (min)
Levels	rotelle	6
	farfalle	14
	shell	22
	hourglass	

	df	sum_sq	mean_sq	F	PR(>F)
C(Shape, Sum)	3	118.0082	39.33606	0.261699	0.851279
C(Tau, Sum)	2	141.4723	70.73614	0.470601	0.63917
C(Shape, Sum):C(Tau, Sum)	6	96.8654	16.14423	0.107406	0.993313
Residual	9	1352.792	150.3103		

**Figure 27:** 2-way ANOVA test examining interactions between shape and residence time on turbidities at 60 min for experiments ran using solution 5, at 0.5” diameter, 96” length, and PETG.

Once again, no significant impact on turbidity is shown, and the P value of all three interactions is significantly higher for this test, at 96” length, than the test with same set of levels except at 48” length, shown in figure 26.

To investigate the effect of tubing length, a slight alteration to the data is needed. An experiment ran at a residence time of 3 min and an experiment at a residence time of 11 min, with all the other factors held constant, really has two physical parameters changed: the nominal residence time, and the flow rate of the solution. Experiments ran at 48” length used residence times of 3, 7, and 11 min, while experiments ran at 96” length used residence times of 6, 14, and 22 min, such that the flow rate used for a particular shape to achieve a 3 min residence time at 48” is the same as needed to achieve a 6 min residence time at 96”. Therefore, a comparison between an experiment with a 3 min residence time at 48” and an experiment with an 11 min residence time at 48” has different flow rates, while a comparison between an experiment with a 3 min

residence time at 48” and an experiment with a 6 min residence time at 96” has the same flow rates. To account for this, in this analysis instead of overall residence time, the normalized residence time per 48” of tubing was used instead. The resulting 3-way ANOVA examining the effect of shape, residence time per 48” of tubing and length on turbidity at 60 min is conducted for experiments ran with solution 5, at 0.5” diameter and using PETG inserts, is shown in figure 28, while the factors and levels included in this dataset are shown in table 13.

**Table 13:** Table showing the factors and levels for experiments run using solution 5, at 0.5” diameter, and PETG.

Factor	Shape	Tubing length (in)	Residence time per 48 "(min)
Levels	rotelle	48	3
	farfalle	96	7
	shell		11
	hourglass		

	sum_sq	df	F	PR(>F)
Intercept	2293.646	1	14.12462	0.000606
C(Shape, Sum)	389.4214	3	0.799372	0.502382
C(Length, Sum)	820.7167	1	5.054098	0.030786
C(Tau, Sum)	351.8406	2	1.083344	0.34924
C(Shape, Sum):C(Length, Sum)	143.9353	3	0.295459	0.82841
C(Shape, Sum):C(Tau, Sum)	379.6653	6	0.389673	0.880761
C(Length, Sum):C(Tau, Sum)	71.46414	2	0.220044	0.803555
C(Shape, Sum):C(Length, Sum):C(Tau, Sum)	170.5478	6	0.175043	0.981901
Residual	5845.91	36		

**Figure 28:** 3-way ANOVA test examining interactions between shape, tubing length and residence time per 48” length on turbidities at 60 min for experiments run using solution 5, at 0.5” diameter, and PETG.

This analysis shows a statistically significant interaction between measured turbidity at 60 min and tube length. Since there are only two levels for tube length, a simple comparison of means of

turbidity at 60 min, 13.83 for 48” length, and 4.82 for 96” length, shows that 48” produced higher turbidity than 96” by a statistically significant amount for experiments run using solution 5, at 0.5” diameter, and PETG. The most likely explanation for this difference is that precipitation forming in the first 48” of the mixer either redissolves into solution over the second 48”, or, more likely, does not make it out of the static mixer. This is possibly due to the increased residence time allowing larger crystals to form that are more likely to drop out of solution as the fluid conditions keeping the crystals suspended in solution are theoretically unchanged across the lengths.

Moving from 0.5” to 1”, due to the extensively discussed issue with variable solution composition when prepared in different quantities, all experiments were conducted with an 11-min residence time except for one experiment conducted at 7 min for hourglass. This was the only shape in which the standard prepared amount, 6 L of the two constituent solutions, was sufficient to last the full 90 min at the flowrate needed for a 7 min residence time. As a result, residence time cannot be examined at 1” diameter. A 2-way ANOVA test investigating the effects of shape and material on turbidities at 90 min for experiments ran at an 11 min residence time, using solution 5, 1” diameter, and 48” length, is shown in figure 29, while the factors and levels included in this dataset are shown in table 14.

**Table 14:** Table showing the factors and levels for experiments ran at an 11 min residence time, using solution 5, at 1” diameter, and 48” length.

Factor	Shape	Material
Levels	farfalle	PETG
	shell	PC
	hourglass	PP

	df	sum_sq	mean_sq	F	PR(>F)
C(Shape, Sum)	2	669.3346	334.6673	0.482311	0.627974
C(Material, Sum)	2	1746.013	873.0063	1.258148	0.316599
C(Shape, Sum):C(Material, Sum)	4	1157.171	289.2928	0.416919	0.79358
Residual	13	9020.469	693.8822		

**Figure 29:** 2-way ANOVA test examining interactions between shape and material on turbidities at 90 min for experiments ran at an 11 min residence time, using solution 5, at 1” diameter, and 48” length.

This analysis shows no significant 1-way or 2-way interactions at this set of levels.

To investigate the effect of tubing diameter, a 2-way ANOVA looking at the effects of shape and diameter on turbidity at 60 minutes is conducted for all experiments ran at 11 min residence time, using solution 5, PETG and 48” length tubing is conducted, with the results shown in figure 30, while the factors and levels included in this dataset are shown in table 15.

**Table 15:** Table showing the factors and levels for experiments ran at an 11 min residence time, using solution 5, PETG, and 48” length.

Factor	Shape	Tubing diameter (in)
Levels	farfalle	0.5
	shell	1
	hourglass	

	df	sum_sq	mean_sq	F	PR(>F)
C(Shape, Sum)	3	2092.228	697.4094	1.062275	0.396421
C(Diameter, Sum)	1	5282.363	5282.363	8.04595	0.013196
C(Shape, Sum):C(Diameter, Sum)	3	72.11798	24.03933	0.036616	0.990206
Residual	14	9191.341	656.5244		

**Figure 30:** 2-way ANOVA test examining interactions between shape and diameter on turbidities at 60 min for experiments ran at an 11 min residence time, using solution 5, PETG, and 48” length.

This analysis shows a statistically significant interaction between measured turbidity at 60 min and tube diameter. Once again, since there are only two levels of tube diameter, a comparison of the means, 48.41 for 1" diameter, and 7.63 for 0.5" diameter, shows that 1" produced higher turbidity than 0.5" by a statistically significant amount for experiments run at an 11 min residence time, using solution 5, at 48" length, and PETG. This may be due to the increase in surface area of the mixer inserts and the increase in rate of ionic collisions that results from the increase in tubing diameter.

To further investigate individual factors, there are some issues with this data that must be overcome. The root cause of most of these issues is the fact that this data was produced with the primary focus being on improving experimental methodology and reducing variability, rather than producing a full and complete dataset ready for statistical analysis. This has led to, among other issues, the problem of high variability in the number of experiments ran at a certain set of parameters. As previously mentioned, this issue limits the strength of any conclusions drawn from ANOVA analysis. It further creates problems when attempting to run a 2-sample Kolmogorov-Smirnov test. 2-sample Kolmogorov-Smirnov tests are used for this analysis because they have the advantage over the results of a 2-factor Tukey's test of significance of increasing the number of experiments being compared, simplifying the result and lowering the problem of low number of observations at each combination of levels that plagues 2-factor Tukey's tests conducted with this data set. Furthermore, a 2-sample Kolmogorov-Smirnov is a non-parametric test and is therefore preferable for this data that cannot be proved to have equal variance.

For example, to compare the resulting turbidities of individual shapes for experiments performed using solution 5, at 0.5” diameter, 48” length, and PETG, the number of experiments for each combination of shape and residence time is shown in table 16.

**Table 16:** Number of experiments for each combination of shape and residence time using solution 5, at 0.5” diameter, 48” length, and PETG.

Shape	Farfalle	Shell	Hourglass	Rotelle
Residence time (min)				
3	3	3	4	2
7	3	11	3	3
11	1	3	1	1

For a comparison of hourglass and shell, not only does the overall number of experiments vary (8 vs 17, respectively), but more concerningly, the distribution of experiments by residence time vary, with the majority of experiments run at 7 min for shell and 3 min for hourglass. Though the 2-way ANOVA test ran with this data, shown in figure 26, failed to show a statistically significant interaction on turbidity by residence time with a P-value of 0.23, this does not prove that residence time does not affect turbidity, just that it cannot be shown to be supported by statistical analysis that it does. Therefore, to conduct a 2-sample Kolmogorov-Smirnov test with these values without accounting for residence time risks skewing the results and impacting the conclusions drawn. As a result, the results from any test conducted using data across multiple levels of a factor such as residence time or shape can only be used to clarify the conclusions drawn from multi-factor ANOVA analysis.

This combination will first be used to compare the resulting turbidities of individual shapes for experiments ran using solution 5, at 0.5” diameter, 48” length, and PETG. While most combinations of shapes did not produce a result suggestive of different resulting turbidity, rotelle

compared against the other three shapes did produce suggestive results. The results of 2-sample Kolmogorov-Smirnov tests comparing rotelle against each farfalle, shell, and hourglass, are shown in figures 31 through 33.

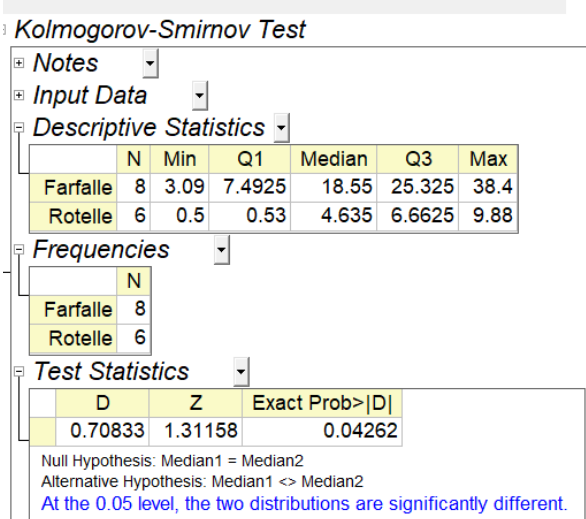


**Figure 31:** 2-sample Kolmogorov-Smirnov tests comparing turbidity at 60 minutes for rotelle and farfalle for experiments ran using solution 5, at 0.5” diameter, 48” length, and PETG.

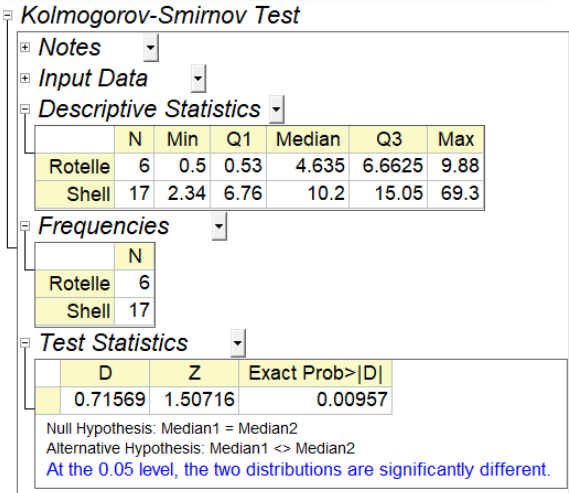


**Figure 32:** 2-sample Kolmogorov-Smirnov tests comparing turbidity at 60 minutes for rotelle and shell for experiments ran using solution 5, at 0.5” diameter, 48” length, and PETG.

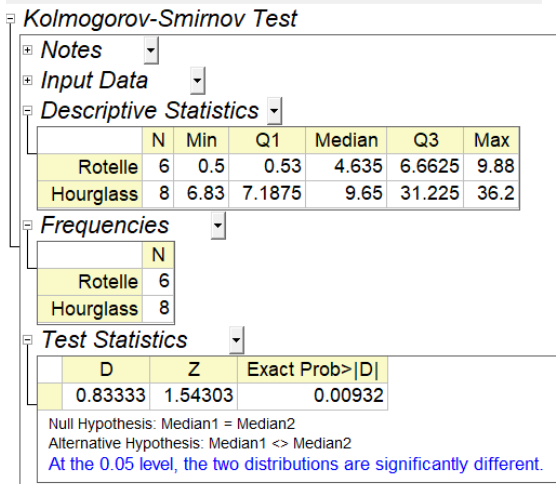


**Figure 33:** 2-sample Kolmogorov-Smirnov tests comparing turbidity at 60 minutes for rotelle and hourglass for experiments ran using solution 5, at 0.5" diameter, 48" length, and PETG.

These results are highly suggestive that all of farfalle, shell and hourglass perform better than rotelle, though the results of the 2-sample ANOVA analysis shown in figure 26 mean that these results are not conclusive.

Finally, individual materials are tested using turbidites at 90 min for experiments ran with an 11 min residence time using solution 5, at 1" diameter, and 48" length. The resulting 2-sample Kolmogorov-Smirnov tests are shown in figures 34-36.

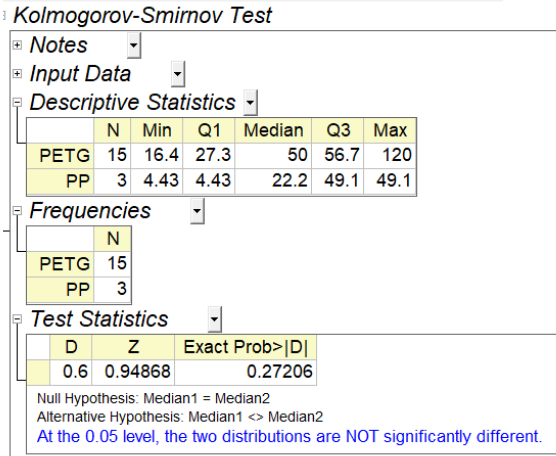


**Figure 34:** 2-sample Kolmogorov-Smirnov tests comparing the turbidity at 90 minutes for PETG and PP for experiments ran with an 11 min residence time using solution 5, at 1" diameter, and 48" length.

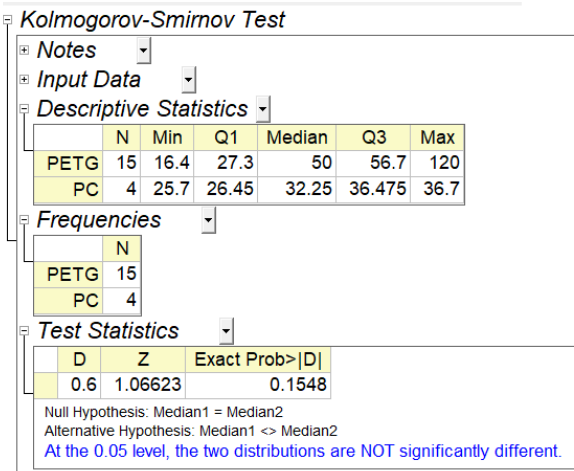


**Figure 35:** 2-sample Kolmogorov-Smirnov tests comparing turbidity at 90 minutes for PETG and PC for experiments ran with an 11 min residence time using solution 5, at 1" diameter, and 48" length.

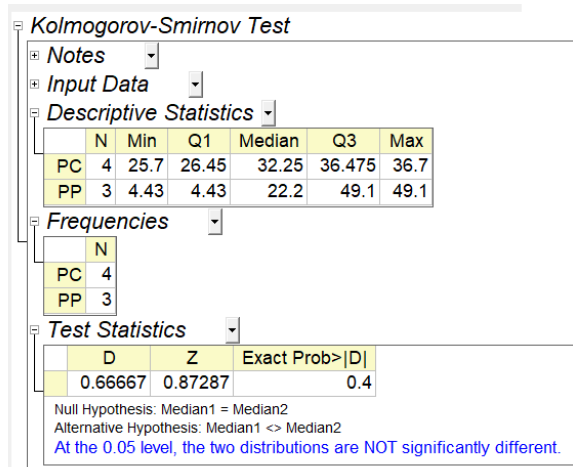


**Figure 36:** 2-sample Kolmogorov-Smirnov tests comparing the turbidity at 90 minutes for PP and PC for experiments ran with an 11 min residence time using solution 5, at 1" diameter, and 48" length.

These results fail to prove anything definitively, but are suggestive that PETG performs better than PC, and are somewhat suggestive that PETG performs better than PP. The strength of these results is severely limited by the low number of experiments run using PC and PP.

### 3.3 Discussion

Any potential conclusions that could be drawn from the data are all limited by the high level of variability in results. Furthermore, the conclusions that can be drawn based on this data must all be considered with the knowledge that all solutions used other than solution 6 have variable compositions due to the difference in atmospheric gas exchange between them. For this reason, after a solution to the variable solution composition problem was devised, no more experiments were run using any solution other than 6. This decision led to some factors, most notably material, producing a highly suggestive result, but falling short of a statistically significant conclusion due to lack of data points. Despite these issues, there are some takeaways from the data.

The first is that the relationship between measured turbidity and depletion calculated from ICP-MS analysis is not as strong as it needs to be to make confident assertions about the effectiveness of this crystallizer based on depletion alone. There are likely several factors limiting the confidence in this relationship. First, as mentioned, human error in sample collection and dilution for ICP-MS analysis could impact the results. It is possible that results produced with procedure 3 and solution 6 show a more clear relationship, as is the case with turbidity and solids collected, but more experiments with the new procedure would need to be run to evaluate this. Next, as also previously mentioned, both the limitations of turbidity as a measure of solids concentrations in solution and scaling and deposition within the static mixer also contribute. For the purposes of this work, not enough data points were produced and had too much variability to use depletion as the primary measurement of interest. Therefore, turbidity must be used, but any conclusions made with these measurements must be taken as suggestive rather than definitive.

No relationship between solids collected and turbidity was found for data produced using procedure 2, while a clear linear, positive relationship is shown in data produced using procedure 3. With these changes, an increased filtration membrane size, and an increased volume of solution being filtered, along with an improved weighing scale and membrane holder, future experiments can use solids collected as a method of evaluation. Furthermore, this result strengthens the conclusions drawn using turbidity, because although solids collected as a method of evaluation has the same issues as turbidity in not accounting for scaling and deposition inside the static mixer, it shows that, for these experiments, turbidity is a reasonable approximation for mass of solids in solution.

Another takeaway is that Kolmogorov mixing length could not be shown to as important as other factors/levels. Though it cannot be said that mixing length has no effect on turbidity or depletion,

the variability between runs of the same parameters is too large and there are too many overlapping effects impacting fluid conditions to isolate any straightforward effects of mixing length. It is possible that future work with improved reproducibility, which investigates more than two diameters, more than two lengths, and a wider number of flow rates and residence times, will be able to isolate and describe the effect of mixing length, but nothing about this relationship could be gained from this work.

There are no significant conclusions to be made about the relationship between residence time and turbidity. One major barrier to reaching a conclusion regarding this relationship is that nearly all experiments at 1" diameter using solution 5 needed to be conducted with an 11 min residence time. This meant that residence time can only be examined using data produced at 0.5" diameter. Though this data is once again limited by high variability and a low number of experiments, and did not produce a statistically significant conclusion, it is suggestive that lower residence times produce higher turbidity. It is possible that the higher mixing energy and flowrates at lower residence times increase the induced turbidity, likely due to an increase in the rate of collisions between ions in solution and nucleation sites, an increase in the rate of critically-sized crystals detaching from nucleation sites to grow in bulk, or some combination of both. If this is the case, then there is likely a "sweet spot" or maximum, past which increasing the flowrate decreases the induced precipitation, as crystals detach from nucleation sites before reaching critical size. These detached crystals would then dissolve back into solution, instead of acting as seed crystals and nucleation sites themselves, inducing precipitation in the bulk solution. However, due to weaknesses in the available data, it is also possible this apparent trend is the result of increased deposition at higher residence times, not lowered induced turbidity. Furthermore, it is possible this trend is unique to 0.5" diameter tubing and does not extend to other diameters. Future work,

using multiple residence times at different diameters, and measuring depletion directly, is needed to draw any meaningful conclusions about this relationship.

While nothing definitive can be said about the effectiveness of hourglass, shell and farfalle against each other, the results are highly suggestive that they all produce higher turbidities than rotelle. It is possible the reduction in variability from using solution 6 will allow future work to reach conclusions regarding these three shapes, but in this work the variability is too high to evaluate them against each other. However, rotelle producing less turbidity than the other three is the strongest conclusion that can be drawn from this work. There are several possible explanations for this result. First, the channels inside the rotelle segregate at least some portion of the solution from the bulk fluid. This could prevent full mixing, and allow pockets of solution that do form critically sized crystals to reach a degree depletion without contributing to depletion of the bulk fluid by acting as nucleation sites. Another possible explanation is that rotelle creates less direct collisions between the solution and the static inserts. Though rotelle provides a larger amount of surface area than the other pieces for the solution to interact with, there is nothing in the shape that creates high energy, orthogonal collisions with the solution. Both shell and hourglass clearly create these collisions, while the “wings” on the farfalle stick out into the bulk solution and create these collisions despite resulting in a lower pressure drop than rotelle. This result has the potential to help reach useful conclusions when paired with computational fluid dynamic simulations. CFD modeling will also allow these two hypotheses to be evaluated to an extent. The results of a cursory investigation into the residence time distribution for the four shapes at a 7 min nominal residence time, 1” diameter and 48” length tubing, using conductivity to measure the concentration of a NaCl solution used as a step input are shown in Appendix D. The results show a significantly lower skewness for rotelle than the other shapes. It is possible

this result shows some characteristic, likely the fact that interior channels of rotelle limit mixing and lateral dispersion, that explains or partially explains the difference in effectiveness, or it could be coincidental. Evaluation of further shapes or CFD modeling of the current shapes is needed to further understand this relationship.

Early in this work, the lack of reproducibility in results was identified as a major obstacle to successfully proving the difference in effectiveness between different factors. As a result, many experiments were run with the same sets of parameters multiple times in an effort to identify sources of inconstancy and improve the procedure and methodology. For example, PETG shell with 7 min residence time, at 0.5” diameter and 48” length was run 17 times for various solutions in an effort to establish a baseline for that set of parameters and evaluate changes to the procedure or the effect of different observations. PETG was used as a baseline for all sets of parameters for this same reason. The consequence of this focus was that experiments using the other two materials of focus, PC and PP, were not run as many times as needed to fully evaluate them against PETG. This, combined with the previously mentioned desire to move away from using solution 5 after the disequilibrium problem was solved, led to both PC and PP having too few data points to create statistically significant conclusions. Despite this lack of statistical certainty, the results suggest that PETG is more effective than either PC or PP. To draw any conclusions about the effect of specific physical characteristics of materials on their effectiveness in inducing turbidity, future work with a wider array of materials is needed.

Though the turbidites resulting from 48” and 96” tubing length are significantly different, at least for 0.5” diameter and using PETG inserts, establishing the cause for this change will require more work. Increased deposition in the longer tube almost certainly plays a role in the lower turbidity. Depletion measurements from future works will help determine how much of this

decreased measured turbidity is attributable to deposition. Future work can further reveal this relationship by conducting experiments at higher flowrates across multiple lengths as increased flowrates will minimize the impact of deposition, increasing the proportion of precipitation that is carried out of the static mixer. Furthermore, experiments using more than two lengths are likely needed to determine a trend in length of tubing. If, by these methods, it is determined that increased deposition does not fully account for the decrease in turbidity at higher tubing lengths, that will be a result that needs to be further explored. It is difficult to identify a theoretical justification to explain this result, as increased residence times combined with higher surface areas should both contribute to higher depletion. This result would also be troubling for this project as a whole, as scaling up of both diameter and length is needed to move to industrial scale.

The statistical analysis of diameter shows that 1" produces statistically significant higher turbidities than 0.5" for experiments performed in 48" tubing length, with an 11 min residence time, and using PETG inserts. This result is consistent with the theory-based predictions for the crystallizer as the increased diameter increases the surface area, and therefore the potential nucleation sites, as well as the rate at which collisions occur between ions. It is promising because of the need to scale-up tubing diameter to move to industrial scale. However, future work done at a wider range of diameters is needed to truly elucidate the relationship between diameter and effectiveness in depletion. Furthermore, future experiments should include multiple residence times and materials, and possibly multiple tubing lengths, to increase the strength and robustness of conclusions to be drawn.

While there are still useful conclusions to be drawn from this work, producing reproducible results was challenging and the focus-shifted to improving the procedure and evaluation

methodology in order to produce the results needed to answer many of the engineering-science questions that were the goal of this work. Additionally, all the results from using solution 5, and the corresponding conclusions, must factor in that the exact solution composition, and therefore the degree of supersaturation, is variable between experiments and impossible to go back and quantify. This factor, combined with the uncertain relationship between measured turbidity and degree of depletion achieved, makes all conclusions from this work suggestive rather than fully demonstrated. While in the end a promising procedure and methodology was developed, its evaluation and use will be in future work. Though it has not been fully evaluated, the procedure and sample solution developed at the end should provide the framework for producing the results needed to produce usable conclusions. Despite these challenges, the results discussed in this section will be helpful in guiding future work.

## Chapter 4

### 4.1 Conclusion

The focus of this work was to evaluate the design parameters of a static mixer crystallizer for use in inducing crystallization in supersaturated brine streams from inland desalination processes.

Model brine solutions are created by mixing two solutions together such that the resulting solution is supersaturated for calcite, and for certain solutions, gypsum as well. This model solution was then pumped through the static mixer and the resulting turbidities, solids in solution, and calcium ion concentrations were measured to try to determine the degree of depletion achieved. The factors/levels evaluated are four shapes of static mixer inserts, farfalle, hourglass, shell and rotelle; 3 materials of inserts, PETG, PC and PP; tubing/pipe diameters of 0.5" and 1"; pipe lengths of 48" and 96"; and nominal residence times of 3, 7, and 11 min (6, 14, and 22 min for 96" pipe). From the earliest experiments, variability and lack of reproducibility of results proved to be a major barrier to successful evaluation of these factors. Much of the focus of this work was on improving the experimental procedure and methodology to reduce the variability and increase the strength of conclusions drawn from the results. This led to six different model solutions being developed, as well as three different experimental procedures. The last procedure and model solution developed showed promising results, but complete studies were left to future work. The experimental results did show that rotelle performs worse than farfalle, hourglass and shell, as well as indicating that a pipe diameter of 1" performs better than 0.5". The results further suggest that mixer inserts made from PETG performs better than PC or PP. The results also showed higher turbidities for 48" length than 96" length, but this is likely due to solids settling in the static mixer. All of the takeaways from these results are limited not only by the variability in results, but also by the lack of a direct relationship between measured

turbidity, used to evaluate experimental results, and degree of depletion achieved, the true figure-of-merit to be evaluated. This was due to flawed experimental protocols that corrupted the latter samples. Furthermore, the data used to produce all conclusions was obtained from experiments using a solution that had a variable and unknown exact composition, to a degree. This means that one of the assumptions made for data analysis, that two experiments run with the same solution components had the same composition, was false. Though this does not mean that the conclusions drawn from the data are incorrect, further evaluation with a model solution of stable composition, such as solution 6, the last solution developed in this work, is needed to draw truly statistically meaningful conclusions.

## **4.2 Future work**

As mentioned, evaluation of the last solution and procedure developed will be important to determining the correct way forward on this project. Despite the major issues in the experimental procedure used to generate most of the data analyzed in this work, and the fact that many experiments were run with the goal of improving the procedure rather than using a set of parameters chosen for the impact that data point would have on the overall narrative, some substantive conclusions can still be drawn. This makes it likely that, even in the worst-case scenario, data producing substantive conclusions can be generated using the updated procedure. However, the number of experiments needed to produce the amount of data needed to generate conclusions could vary greatly depending on the reproducibility of results generated. The number of experiments is of crucial importance given the costs associated with running an experiment. A single experiment, from start to finish, can take up to 4 h, in addition to the cost of materials and instrumentation. Therefore, evaluation of the updated procedure is needed to determine the feasibility of continuing with benchtop, batch experimentation.

One further change that should be made to the procedure is to include measurements of pH and calcium ion concentration using an ion selective probe. Depending on the amount of time and volume of sample needed for the instrumentation to produce a reading, some care will need to be taken to ensure that varying flowrates don't change the amount of time between the solution leaving the static mixer and the reading being taken, as continued crystallization in that time could impact the results.

Of the results generated in this work, investigating different materials seems to offer the highest confidence. Even using the flawed procedure 2, it seems likely that with just a few more data points for PC and PP, substantive conclusions could be drawn. All the other factors examined work together and affect one another to create a unique set of fluid conditions. Creating a narrative from the results of just one of these factors will be difficult, and there is not a straightforward path to identifying and separating one measure of fluid conditions to assess its impact. For example, to investigate residence times by changing the flow rates necessarily changes many fluid conditions beyond just nominal residence time, including Kolmogorov mixing length and many of the characteristic fluid transport parameters. Varying material, in contrast, does not physically interact with any of the other factors, and fluid conditions, and the various metrics used to quantify fluid conditions can be held constant despite the variable material. The lack of complicating factors means investigating the relationship between effectiveness in inducing nucleation and crystallization and the specific physical characteristics of a material could produce an interesting, useful, and conclusive result. Future work using computational fluid dynamics (CFD) to try to simplify the overlapping factors impacting fluid conditions may provide some insight into the impact of various aspects of fluid conditions on induced crystallizations, but the strength of conclusions drawn remains to be seen.

The physical characteristics that may affect induced precipitation and will need to be evaluated for the various materials, vary widely. At a molecular or surface chemistry level scale, related but distinct characteristics such as a materials charge, polarity, hydrophobicity, specific functional groups, and roughness could all potentially play a role in the precipitation of calcite. These characteristics are theoretically constant for a given material regardless of what form it is measured in (i.e., specific brand of 3-d printing filament, extrudable pellets vs thin film, etc.). At a larger scale, the macroscopic characteristics of a material governed by the specific way the material used reacts to being extruded and hardened in the 3-d printing process, particularly roughness, could have an impact. Though the underlying chemistry clearly still plays a role at this scale, the properties of the specific polymer used to produce the printed filament also impacts this scale of roughness. Finally, at the largest scale, the specific characteristics of a printed insert based on the way each printed layer adheres and reacts to the layer above and below it could also be important. These characteristics, which once again can be roughly categorized and quantified as “roughness”, are impacted by the settings of the printer, as well as the specific filament used and the material’s chemistry.

Some of these characteristics, such as the properties of a material’s functional groups or a material’s polarity, have been well explored in literature, or can be derived from existing measurements and theory. Other characteristics, such as all three scales of roughness and hydrophobicity, may be available for some materials, but will mostly need to be evaluated for specific elements produced. While a methodology for establishing a surface's hydrophobicity is well established, the quantification of roughness may require fine tuning<sup>58</sup>. Atomic force microscopy can be used to quantify the molecular level roughness, while the method for

establishing roughness at the two higher scales will depend on the instrumentation available and may require some further exploration<sup>59</sup>.

While a variety of polymers should be evaluated, one in particular, the polymer EVOH-E, a form of ethylene-vinyl alcohol copolymer, should be investigated due to a previous study from the group that used a “shaken jar” experiment to investigate the impact of various polymer surfaces on the crystallization of calcite<sup>52</sup>. In that study, a solution supersaturated for calcite is placed in jar and placed on a shaking table apparatus for a period of time. They found that EVOH-E promoted crystallization while also remaining resistant to scaling or deposition of solids onto the surface of the polymer. These two characteristics make EVOH-E an ideal candidate for this use in the static mixer.

Finally, some of the major challenges in this work can be overcome by future work directly using brine produced by reverse osmosis filtration. Though substantial logistical issues will need to be overcome to integrate the static mixer into an existing desalination apparatus and put in place a system for monitoring inflow solution composition if one does not already exist, using a direct connection to a brine supply will avoid many of the challenges that plagued this work. To begin, the scale of brine available will allow longer term experiments than can be conducted with model solutions created in the lab. This means that data can be produced closer to steady state, away from the unpredictability of start-up conditions, thus reducing variability. Additionally, larger sized static mixers and higher flowrates may be available for exploration. The increased amount of solution available also means that it is feasible to take turbidity and other measurements inline, where at lower volumes they need to be done by waiting for a sample large enough to produce a measurement. The combination of easier measurements and longer experiments should allow more reproducible data, and, combined with not needing to prepare the model solutions,

lower the amount of work needed to run one experiment. This method may, however, come with its own set of unforeseen challenges even after the high up-front cost, so the most effective and efficient combination of benchtop and field experiments remains to be seen. Regardless of the exact methods used, it is still likely that material will yield the most efficient results.

## Bibliography

- (1) Xu, X.; Ness, J. E.; Miara, A.; Sitterley, K. A.; Talmadge, M.; O'Neill, B.; Coughlin, K.; Akar, S.; Edirisooriya, E. M. N. T.; Kurup, P.; Rao, N.; Macknick, J.; Stokes-Draut, J. R.; Xu, P. Analysis of Brackish Water Desalination for Municipal Uses: Case Studies on Challenges and Opportunities. *ACS EST Eng.* **2022**, *2* (3), 306–322. <https://doi.org/10.1021/acsestengg.1c00326>.
- (2) Khan, Q.; Maraqa, M. A.; Mohamed, A.-M. O. Chapter 17 - Inland Desalination: Techniques, Brine Management, and Environmental Concerns. In *Pollution Assessment for Sustainable Practices in Applied Sciences and Engineering*; Mohamed, A.-M. O., Paleologos, E. K., Howari, F. M., Eds.; Butterworth-Heinemann, **2021**; pp 871–918. <https://doi.org/10.1016/B978-0-12-809582-9.00017-7>.
- (3) Tang, X.; Kum, S.; Liu, H. Inland Desalination Brine Disposal: A Baseline Study from Southern California on Brine Transport Infrastructure and Treatment Potential. *ACS EST Eng.* **2022**, *2* (3), 456–464. <https://doi.org/10.1021/acsestengg.1c00276>.
- (4) Badruzzaman, M.; Oppenheimer, J.; Adham, S.; Kumar, M. Innovative Beneficial Reuse of Reverse Osmosis Concentrate Using Bipolar Membrane Electrodialysis and Electrochlorination Processes. *J. Membr. Sci.* **2009**, *326* (2), 392–399. <https://doi.org/10.1016/j.memsci.2008.10.018>.
- (5) Buros, O.K. The ABCs of Desaltig. *International Desalination Association*. **2000**.
- (6) Mohamed, A. M. O.; Maraqa, M.; Al Handhaly, J. Impact of Land Disposal of Reject Brine from Desalination Plants on Soil and Groundwater. *Desalination* **2005**, *182* (1), 411–433. <https://doi.org/10.1016/j.desal.2005.02.035>.
- (7) Mickley, A. Updated and Extended Survey of U.S. Municipal Desalination Plants. *Desalination and Water Purification Research and Development Program Report No. 207* **2018**.
- (8) Zhang, C.; Shi, Y.; Shi, L.; Li, H.; Li, R.; Hong, S.; Zhuo, S.; Zhang, T.; Wang, P. Designing a next Generation Solar Crystallizer for Real Seawater Brine Treatment with Zero Liquid Discharge. *Nat. Commun.* **2021**, *12* (1), 998. <https://doi.org/10.1038/s41467-021-21124-4>.
- (9) Vane, L. M.; Rock, K.; Jordan, D. Energy Efficient Vortex-Enhanced Water Evaporation Technology for Concentrated Brine Management: Theory and Process Simulation Evaluation. *Desalination* **2022**, *522*, 115427. <https://doi.org/10.1016/j.desal.2021.115427>.
- (10) Gu, R.; Yu, Z.; Sun, Y.; Su, Y.; Wu, W.; Cheng, S. Janus 3D Solar Crystallizer Enabling an Eco-Friendly Zero Liquid Discharge of High-Salinity Concentrated Seawater with Antiscalant. *Desalination* **2022**, *537*, 115862. <https://doi.org/10.1016/j.desal.2022.115862>.
- (11) Yin, Q.; Kong, F.; Wang, S.; Du, J.; Pan, L.; Tao, Y.; Li, P. 3D Printing of Solar Crystallizer with Polylactic Acid/Carbon Composites for Zero Liquid Discharge of High-Salinity Brine. *Polymers* **2023**, *15* (7), 1656. <https://doi.org/10.3390/polym15071656>.
- (12) Liu, J.; Wang, Y.; Li, Z.; Liu, X.; Li, W. Flux Decline Induced by Scaling of Calcium Sulfate in Membrane Distillation: Theoretical Analysis on the Role of Different Mechanisms. *J. Membr. Sci.* **2021**, *628*, 119257. <https://doi.org/10.1016/j.memsci.2021.119257>.
- (13) Shmulevsky, M.; Li, X.; Shemer, H.; Hasson, D.; Semiat, R. Analysis of the Onset of Calcium Sulfate Scaling on RO Membranes. *J. Membr. Sci.* **2017**, *524*, 299–304. <https://doi.org/10.1016/j.memsci.2016.11.055>.

- (14) Matin, A.; Rahman, F.; Shafi, H. Z.; Zubair, S. M. Scaling of Reverse Osmosis Membranes Used in Water Desalination: Phenomena, Impact, and Control; Future Directions. *Desalination* **2019**, *455*, 135–157. <https://doi.org/10.1016/j.desal.2018.12.009>.
- (15) Choi, J. Y.; Kaufmann, F.; Rahardianto, A.; Cohen, Y. Desupersaturation of RO Concentrate and Gypsum Removal via Seeded Precipitation in a Fluidized Bed Crystallizer. *Water Res.* **2021**, *190*, 116766. <https://doi.org/10.1016/j.watres.2020.116766>.
- (16) McCool, B. C.; Rahardianto, A.; Cohen, Y. Antiscalant Removal in Accelerated Desupersaturation of RO Concentrate via Chemically-Enhanced Seeded Precipitation (CESP). *Water Res.* **2012**, *46* (13), 4261–4271. <https://doi.org/10.1016/j.watres.2012.04.045>.
- (17) Sancio, P.; Ostarcevic, E.; Atherton, P.; Leslie, G.; Fane, T.; Cohen, Y.; Payne, M.; Gray, S. Enhancement of Reverse Osmosis Water Recovery Using Interstage Calcium Precipitation. *Desalination* **2012**, *295*, 43–52. <https://doi.org/10.1016/j.desal.2012.03.015>.
- (18) McCool, B. C.; Rahardianto, A.; Faria, J. I.; Cohen, Y. Evaluation of Chemically-Enhanced Seeded Precipitation of RO Concentrate for High Recovery Desalting of High Salinity Brackish Water. *Desalination* **2013**, *317*, 116–126. <https://doi.org/10.1016/j.desal.2013.01.010>.
- (19) Mahvi, A. H.; Shafiee, F.; Naddafi, K. Feasibility Study of Crystallization Process for Water Softening in a Pellet Reactor. *Int. J. Environ. Sci. Technol.* **2005**, *1* (4), 301–304. <https://doi.org/10.1007/BF03325846>.
- (20) Rahardianto, A.; Gao, J.; Gabelich, C. J.; Williams, M. D.; Cohen, Y. High Recovery Membrane Desalting of Low-Salinity Brackish Water: Integration of Accelerated Precipitation Softening with Membrane RO. *J. Membr. Sci.* **2007**, *289* (1), 123–137. <https://doi.org/10.1016/j.memsci.2006.11.043>.
- (21) Halevy, S.; Korin, E.; Gilron, J. Kinetics of Gypsum Precipitation for Designing Interstage Crystallizers for Concentrate in High Recovery Reverse Osmosis. *Ind. Eng. Chem. Res.* **2013**, *52* (41), 14647–14657. <https://doi.org/10.1021/ie400977p>.
- (22) Gabelich, C. J.; Rahardianto, A.; Northrup, C. R.; Yun, T. I.; Cohen, Y. Process Evaluation of Intermediate Chemical Demineralization for Water Recovery Enhancement in Production-Scale Brackish Water Desalting. *Desalination* **2011**, *272* (1), 36–45. <https://doi.org/10.1016/j.desal.2010.12.050>.
- (23) Tran, A. T. K.; Zhang, Y.; Jullok, N.; Meesschaert, B.; Pinoy, L.; Van der Bruggen, B. RO Concentrate Treatment by a Hybrid System Consisting of a Pellet Reactor and Electrodialysis. *Chem. Eng. Sci.* **2012**, *79*, 228–238. <https://doi.org/10.1016/j.ces.2012.06.001>.
- (24) Ravichandran, S. A.; Krist, J.; Edwards, D.; Delagah, S.; Pellegrino, J. Measuring Sparingly-Soluble, Aqueous Salt Crystallization Kinetics Using CSTRs-in-Series: Methodology Development and CaCO<sub>3</sub> Studies. *Sep. Purif. Technol.* **2019**, *211*, 408–420. <https://doi.org/10.1016/j.seppur.2018.09.084>.
- (25) Thakur, R. K.; Vial, C.; Nigam, K. D. P.; Nauman, E. B.; Djelveh, G. STATIC MIXERS IN THE PROCESS INDUSTRIES DA REVIEW. **2003**, *81*.
- (26) Kelton, K. F.; Greer, A. L. Chapter 2 - The Classical Theory. In *Pergamon Materials Series*; Kelton, K. F., Greer, A. L., Eds.; Nucleation in Condensed Matter; Pergamon, 2010; Vol. 15, pp 19–54. [https://doi.org/10.1016/S1470-1804\(09\)01502-8](https://doi.org/10.1016/S1470-1804(09)01502-8).

- (27) Nanev, C. N. 7 - Theory of Nucleation. In *Handbook of Crystal Growth (Second Edition)*; Nishinaga, T., Ed.; Elsevier: Boston, 2015; pp 315–358. <https://doi.org/10.1016/B978-0-444-56369-9.00007-1>.
- (28) Pritula, I.; Sangwal, K. 29 - Fundamentals of Crystal Growth from Solutions. In *Handbook of Crystal Growth (Second Edition)*; Rudolph, P., Ed.; Handbook of Crystal Growth; Elsevier: Boston, 2015; pp 1185–1227. <https://doi.org/10.1016/B978-0-444-63303-3.00029-8>.
- (29) ter Horst, J. H.; Schmidt, C.; Ulrich, J. 32 - Fundamentals of Industrial Crystallization. In *Handbook of Crystal Growth (Second Edition)*; Rudolph, P., Ed.; Handbook of Crystal Growth; Elsevier: Boston, 2015; pp 1317–1349. <https://doi.org/10.1016/B978-0-444-63303-3.00032-8>.
- (30) Three-Dimensional Nucleation and Metastable Zone Width. In *Additives and Crystallization Processes*; John Wiley & Sons, Ltd, 2007; pp 21–63. <https://doi.org/10.1002/9780470517833.ch2>.
- (31) Uwaha, M. 8 - Growth Kinetics: Basics of Crystal Growth Mechanisms. In *Handbook of Crystal Growth (Second Edition)*; Nishinaga, T., Ed.; Elsevier: Boston, 2015; pp 359–399. <https://doi.org/10.1016/B978-0-444-56369-9.00008-3>.
- (32) Kelton, K. F.; Greer, A. L. Chapter 6 - Heterogeneous Nucleation. In *Pergamon Materials Series*; Kelton, K. F., Greer, A. L., Eds.; Nucleation in Condensed Matter; Pergamon, 2010; Vol. 15, pp 165–226. [https://doi.org/10.1016/S1470-1804\(09\)01506-5](https://doi.org/10.1016/S1470-1804(09)01506-5).
- (33) Dong, Y.; Ng, W. K.; Hu, J.; Shen, S.; Tan, R. B. H. A Continuous and Highly Effective Static Mixing Process for Antisolvent Precipitation of Nanoparticles of Poorly Water-Soluble Drugs. *Int. J. Pharm.* **2010**, *386* (1), 256–261. <https://doi.org/10.1016/j.ijpharm.2009.11.007>.
- (34) Alvarez, A. J.; Myerson, A. S. Continuous Plug Flow Crystallization of Pharmaceutical Compounds. *Cryst. Growth Des.* **2010**, *10* (5), 2219–2228. <https://doi.org/10.1021/cg901496s>.
- (35) Mathew Thomas, K.; Nyande, B. W.; Lakerveld, R. Design and Characterization of Kenics Static Mixer Crystallizers. *Chem. Eng. Res. Des.* **2022**, *179*, 549–563. <https://doi.org/10.1016/j.cherd.2022.01.025>.
- (36) Dong, Y.; Ng, W. K.; Shen, S.; Kim, S.; Tan, R. B. H. Solid Lipid Nanoparticles: Continuous and Potential Large-Scale Nanoprecipitation Production in Static Mixers. *Colloids Surf. B Biointerfaces* **2012**, *94*, 68–72. <https://doi.org/10.1016/j.colsurfb.2012.01.018>.
- (37) Douroumis, D.; Scheler, S.; Fahr, A. Using a Modified Shepards Method for Optimization of a Nanoparticulate Cyclosporine a Formulation Prepared by a Static Mixer Technique. *J. Pharm. Sci.* **2008**, *97* (2), 919–930. <https://doi.org/10.1002/jps.21001>.
- (38) Majumder, A.; Nagy, Z. K.; Ni, X.-W. Recent Advances in Continuous Crystallization. *Chem. Eng. Res. Des.* **2022**, *186*, 610–613. <https://doi.org/10.1016/j.cherd.2022.08.028>.
- (39) Stec, M.; Synowiec, P. M. Study of Fluid Dynamic Conditions in the Selected Static Mixers Part I- Research of Pressure Drop. *Can. J. Chem. Eng.* **2017**, *95* (11), 2156–2167. <https://doi.org/10.1002/cjce.22929>.
- (40) Synowiec, P. M.; Stec, M. Analysis of CaF<sub>2</sub> Precipitation Process in the Selected Static Mixers. *J. Chem.* **2019**, *2019*, e6728492. <https://doi.org/10.1155/2019/6728492>.

- (41) Amores, I. D.; González-Gutiérrez, J.; García, I. M.; Franco, J. M.; Gallegos, C. 3D Printing – Present and Future – A Chemical Engineering Perspective. *Chem. Eng. Res. Des.* **2022**, *187*, 598–610. <https://doi.org/10.1016/j.cherd.2022.08.049>.
- (42) Kundra, M.; Zhu, Y.; Nguyen, X.; Fraser, D.; Hornung, C. H.; Tsanaksidis, J. 3D Printed Nickel Catalytic Static Mixers Made by Corrosive Chemical Treatment for Use in Continuous Flow Hydrogenation. *React. Chem. Eng.* **2022**, *7* (2), 284–296. <https://doi.org/10.1039/D1RE00456E>.
- (43) Percin, K.; Rommerskirchen, A.; Sengpiel, R.; Gendel, Y.; Wessling, M. 3D-Printed Conductive Static Mixers Enable All-Vanadium Redox Flow Battery Using Slurry Electrodes. *J. Power Sources* **2018**, *379*, 228–233. <https://doi.org/10.1016/j.jpowsour.2018.01.061>.
- (44) Kundra, M.; Grall, T.; Ng, D.; Xie, Z.; Hornung, C. H. Continuous Flow Hydrogenation of Flavorings and Fragrances Using 3D-Printed Catalytic Static Mixers. *Ind. Eng. Chem. Res.* **2021**, *60* (5), 1989–2002. <https://doi.org/10.1021/acs.iecr.0c05671>.
- (45) Gutmann, B.; Köckinger, M.; Glotz, G.; Ciaglia, T.; Slama, E.; Zadavec, M.; Pfanner, S.; Maier, M. C.; Gruber-Wölfler, H.; Kappe, C. O. Design and 3D Printing of a Stainless Steel Reactor for Continuous Difluoromethylations Using Fluoroform. *React. Chem. Eng.* **2017**, *2* (6), 919–927. <https://doi.org/10.1039/C7RE00176B>.
- (46) Lebl, R.; Zhu, Y.; Ng, D.; Hornung, C. H.; Cantillo, D.; Kappe, C. O. Scalable Continuous Flow Hydrogenations Using Pd/Al<sub>2</sub>O<sub>3</sub>-Coated Rectangular Cross-Section 3D-Printed Static Mixers. *Catal. Today* **2022**, *383*, 55–63. <https://doi.org/10.1016/j.cattod.2020.07.046>.
- (47) Lemanowicz, M.; Mielńczyk, A.; Walica, T.; Kotek, M.; Gierczycki, A. Application of Polymers as a Tool in Crystallization—A Review. *Polymers* **2021**, *13* (16), 2695. <https://doi.org/10.3390/polym13162695>.
- (48) Dalas, E. Crystallization of Sparingly Soluble Salts on Functionalized Polymers. *J. Mater. Chem.* **1991**, *1* (3), 473–474. <https://doi.org/10.1039/JM9910100473>.
- (49) Frank, D. S.; Matzger, A. J. Influence of Chemical Functionality on the Rate of Polymer-Induced Heteronucleation. *Cryst. Growth Des.* **2017**, *17* (8), 4056–4059. <https://doi.org/10.1021/acs.cgd.7b00593>.
- (50) Diao, Y.; Helgeson, M. E.; Siam, Z. A.; Doyle, P. S.; Myerson, A. S.; Hatton, T. A.; Trout, B. L. Nucleation under Soft Confinement: Role of Polymer–Solute Interactions. *Cryst. Growth Des.* **2012**, *12* (1), 508–517. <https://doi.org/10.1021/cg201434r>.
- (51) Curcio, E.; López-Mejías, V.; Di Profio, G.; Fontananova, E.; Drioli, E.; Trout, B. L.; Myerson, A. S. Regulating Nucleation Kinetics through Molecular Interactions at the Polymer–Solute Interface. *Cryst. Growth Des.* **2014**, *14* (2), 678–686. <https://doi.org/10.1021/cg4015543>.
- (52) Hutfles, J.; Ravichandran, S. A.; Pellegrino, J. Screening Polymer Surfaces in Crystallization. *Colloids Surf. Physicochem. Eng. Asp.* **2019**, *582*, 123869. <https://doi.org/10.1016/j.colsurfa.2019.123869>.
- (53) Yin, Y.; Li, T.; Zuo, K.; Liu, X.; Lin, S.; Yao, Y.; Tong, T. Which Surface Is More Scaling Resistant? A Closer Look at Nucleation Theories for Heterogeneous Gypsum Nucleation in Aqueous Solutions. *Environ. Sci. Technol.* **2022**, *56* (22), 16315–16324. <https://doi.org/10.1021/acs.est.2c06560>.
- (54) Patel, M. A.; Nguyen, B.; Chadwick, K. Predicting the Nucleation Induction Time Based on Preferred Intermolecular Interactions. *Cryst. Growth Des.* **2017**, *17* (9), 4613–4621. <https://doi.org/10.1021/acs.cgd.7b00446>.

- (55) M. Schall, J.; Capellades, G.; S. Myerson, A. Methods for Estimating Supersaturation in Antisolvent Crystallization Systems. *CrystEngComm* **2019**, *21* (38), 5811–5817. <https://doi.org/10.1039/C9CE00843H>.
- (56) *Hypothesis Testing - Analysis of Variance (ANOVA)*. [https://sphweb.bumc.bu.edu/otlt/mph-modules/bs/bs704\\_hypothesistesting-anova/bs704\\_hypothesistesting-anova\\_print.html](https://sphweb.bumc.bu.edu/otlt/mph-modules/bs/bs704_hypothesistesting-anova/bs704_hypothesistesting-anova_print.html) (accessed 2023-11-30).
- (57) Pratt, J. W.; Gibbons, J. D. Kolmogorov-Smirnov Two-Sample Tests. In *Concepts of Nonparametric Theory*; Springer Series in Statistics; Springer New York: New York, NY, 1981; pp 318–344. [https://doi.org/10.1007/978-1-4612-5931-2\\_7](https://doi.org/10.1007/978-1-4612-5931-2_7).
- (58) Huang, X.; Li, C.; Zuo, K.; Li, Q. Predominant Effect of Material Surface Hydrophobicity on Gypsum Scale Formation. *Environ. Sci. Technol.* **2020**, *54* (23), 15395–15404. <https://doi.org/10.1021/acs.est.0c03826>.
- (59) Lin, N. H.; Shih, W.-Y.; Lyster, E.; Cohen, Y. Crystallization of Calcium Sulfate on Polymeric Surfaces. *J. Colloid Interface Sci.* **2011**, *356* (2), 790–797. <https://doi.org/10.1016/j.jcis.2011.01.042>.

## Appendices

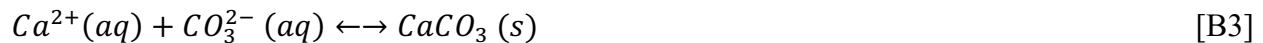
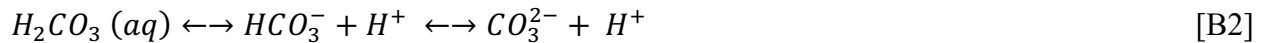
### A. Summary of procedures

Table A1: Summary of the three procedure used in this work.

	Sampling	Filtration amount	Filtration apparatus
Procedure 1	No sampling	N/A	N/A
Procedure 2	Sampling at inflow at 20, 40, 60 and 80 min and outflow at 30, 60 and 90 min	20 mL	25 mm Cole-Parmer syringe filter holder
Procedure 3	Sampling at outflow at 30, 60, and 90 min, and of unmixed solution at start of experiment	100 mL	47 mm Sartorius In-Line Stainless Steel Filter Holder

## B. Prepared solution disequilibrium

The equations governing calcite formation and carbonate systems, shown in equations 2-4 in section 1.1, are copied below for simplicity.



The original procedure called for two solutions to be mixed, then set out overnight with the lids open to allow air, specifically CO<sub>2</sub> to interact with the solution. The assumption was that by leaving the containers open overnight, and giving the solutions 16-24 hours to equilibrate, the carbonate ions in solution and atmospheric CO<sub>2</sub> will reach an equilibrium, as CO<sub>2</sub> either leave or enters the solution in the form of equation B1.

However, while this assumption was true for solution 1, as the supersaturation index was increased in later solutions, this assumption broke down. As the amount of NaHCO<sub>3</sub> was increased, the amount of time necessary to reach equilibrium increased as the necessary amount of carbonate to leave the system increased. The issue became apparent when changing the volumes of solutions produced and a given time. To conduct one experiment with a residence time of 11 minutes at 1" diameter, producing 6 L of each solution is enough. However, to run experiments at lower residence times, or conduct more than one experiment in a day, higher volumes of solution need to be produced. If the solutions were getting to an equilibrium point in the 16-24 hours of atmospheric interaction time, the compositions of the solutions at the time of the experiment would be the same, and the resulting turbidity measurements at the same

parameters would be consistent regardless of the volumes of solution produced. However, what was observed was a difference in resulting turbidities well outside the normal variability.

Two different sets of experiments were run with identical parameters, varying only the volume of the solutions prepared. In other words, the same experiments were run with the same solutions, mixed in tubs of the same diameters, with the only difference being the volume of water and mass of salts combined to create the solutions, with the resulting solutions having identical compositions before any interaction with atmospheric gasses can occur. The results are summarized in tables B1 and B2.

**Table B1:** Experiments conducted at 1” diameter, shape of Farfalle, material of PETG, 48” length, 11-minute residence time, and solution 11. Turbidity values are average of turbidity readings taken at 90 minutes.

Volume of solution prepared	# of runs	Turbidity (NTU)	Standard deviation of turbidity	Conductivity (mS)	Temperature (C)	Pressure (PSI)
6 L	5	36.34	13.78	17.07	19.1	.2166
12 L	3	2.80	1.30	17.81	19.8	.2491
18 L	1	1.91	na	17.64	19.3	.3348

**Table B2:** Experiments conducted at 1” diameter, shape of Hourglass, material of PETG, 48” length, 11-minute residence time, and solution 11. Turbidity values are average of turbidity readings taken at 90 minutes.

Volume of solution prepared	# of runs	Turbidity (NTU)	Standard deviation of turbidity	Conductivity (mS)	Temperature (C)	Pressure (PSI)
6 L	4	56.03	16.48	17.48	20.8	.2429
12 L	1	9.94	na	17.39	21.0	.2546

The major takeaway from these experiments was that experiments conducted using solutions produced in 6 L batches resulted in significantly higher turbidity readings when compared to either experiments using either 12 L or 18 L solution volumes. This led to the conclusion that some change in composition of the solutions was happening differently based on either the change in overall volume of the solutions, or the change in the surface area to volume ratio as they interacted with atmospheric gasses, as the surface area exposed to the atmosphere stayed the same and the volume changed. One obvious consequence of this changing surface area to volume ratio was that as water evaporated from the solutions, since the surface area exposed did not change with the volume, the evaporation rates stayed the same. With the differing volumes, however, the compositions of the solutions changed at different rates, with, for example, the amount of water lost to evaporation after 24 hours being a higher percentage of the overall water for a 6 L batch, resulting in a more concentrated solution, and ultimately a higher degree of supersaturation. To test this, the amount of water lost to evaporation after 24 hours was determined to be around 140 mL, and a solution was made using 11.86 L of water, instead of 12

L. This meant that after 24 hours of evaporation, the 12 L solutions were proportionally the same concentration as a 6 L solution would be. The solution with evaporation accounted for was run with the same parameters as the experiments in table 1, resulting in a turbidity at 90 minutes of 4.29. While with only one experimental run with this solution, it is not possible to say with certainty if accounting for evaporation meaningfully changes the resulting turbidity, it can be said with certainty that evaporation is not the main cause of the difference in resulting turbidities for 6 L batches vs 12 L or 18 L batches shown in tables 1 and 2.

With evaporation eliminated as the main cause of the issue, the other obvious potential cause was that the solutions were not reaching equilibrium with the atmosphere in the 16-24 hours that they were being left open for interaction. Since the interface area of the solutions was the same for all volumes of solution, the rate of exchange is similar for all volumes, despite the total amount of  $\text{CO}_2$  needed to be exchanged being proportional to the volume of solution, changing the volume and not allowing equilibrium to be reached will create solutions with different compositions. Furthermore, while equilibrium may be reached at the interchange surface for both, equilibrium for the entire solution is limited by diffusion of carbonate molecules either to or from the surface. The further distance the carbonate ions need to travel for higher volumes again creates differences in compositions between the solutions if they are not allowed to fully equilibrate.

To test this hypothesis, the pH of the solutions over time were measured. Following equation B1,  $\text{CO}_2$  being absorbed into the solution creates  $\text{H}_2\text{CO}_3$ , while  $\text{CO}_2$  being released into the atmosphere necessarily removes  $\text{H}_2\text{CO}_3$ .  $\text{H}_2\text{CO}_3$  disassociates according to equation B2.

As a result of this disassociation, when  $\text{CO}_2$  is absorbed, it results in the release of hydrogen ions, lowering the pH. Conversely, by Le Chatelier's principle, when  $\text{CO}_2$  is released the concentration

of  $\text{H}_2\text{CO}_3$  is decreased, causing  $\text{HCO}_3^-$  and  $\text{CO}_3^{2-}$  ions to associate with hydrogen ions, removing them from the solution and raising the pH. Based on this theory, if a solution's pH is changing, gas exchange is happening, and if a pH is constant then no exchange is occurring, and equilibrium is reached. The two constituent solutions of solution 5 are prepared in 6 L batches, then left with the lid open, and the pH of both are taken over 5-minute intervals. The results of these experiments are shown in figures B1 and B2.

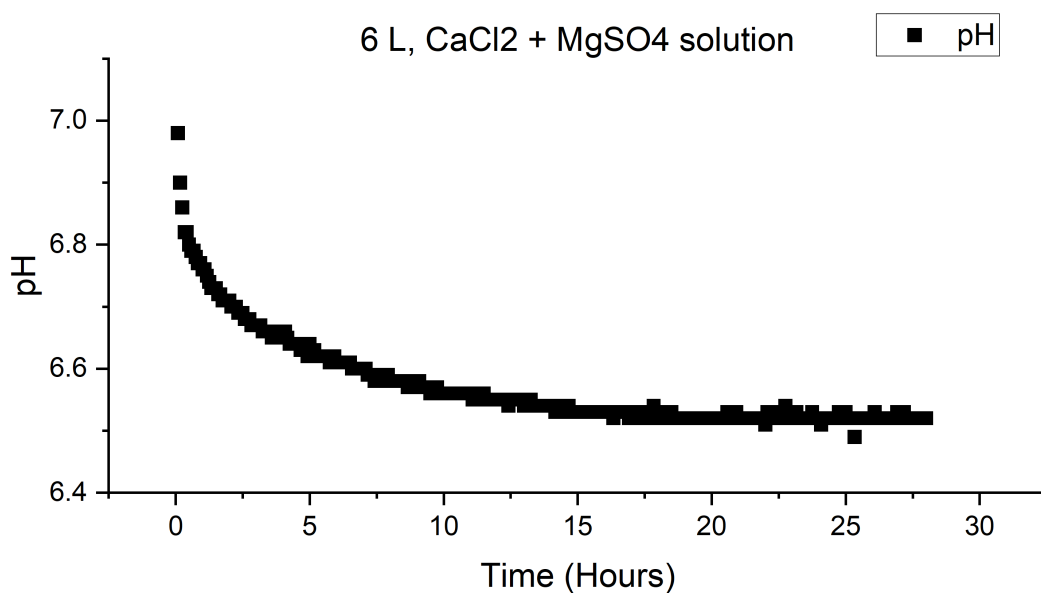


**Figure B1:** pH over time for 6 L of solution 5A left open to atmosphere.

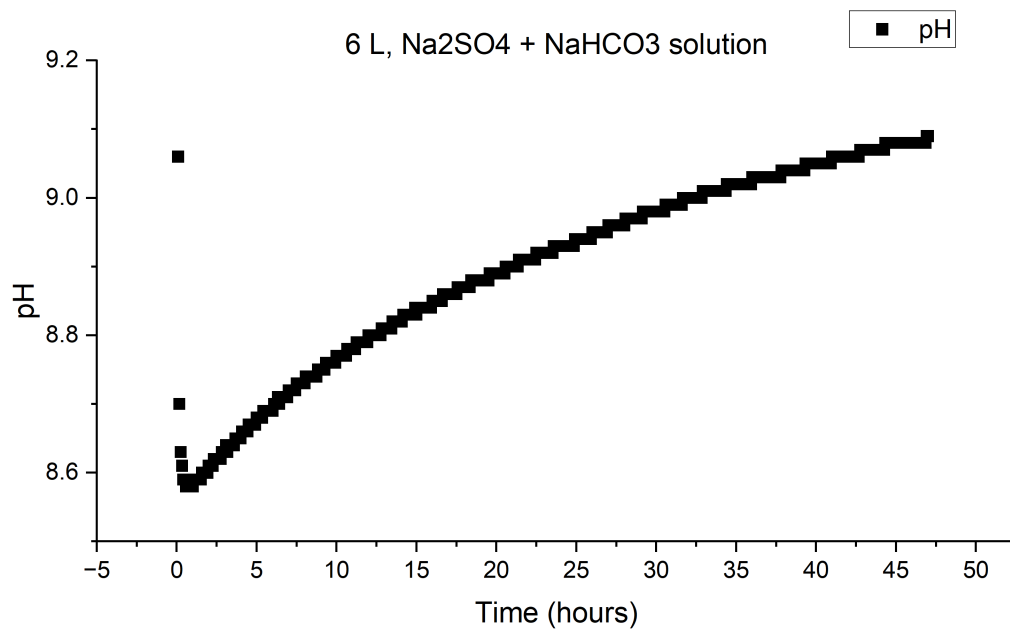


**Figure B2:** pH over time for 6 L of solution 5B left open to atmosphere.

The same experiment is then run with 12 L batches, shown in figure B3 and B4.

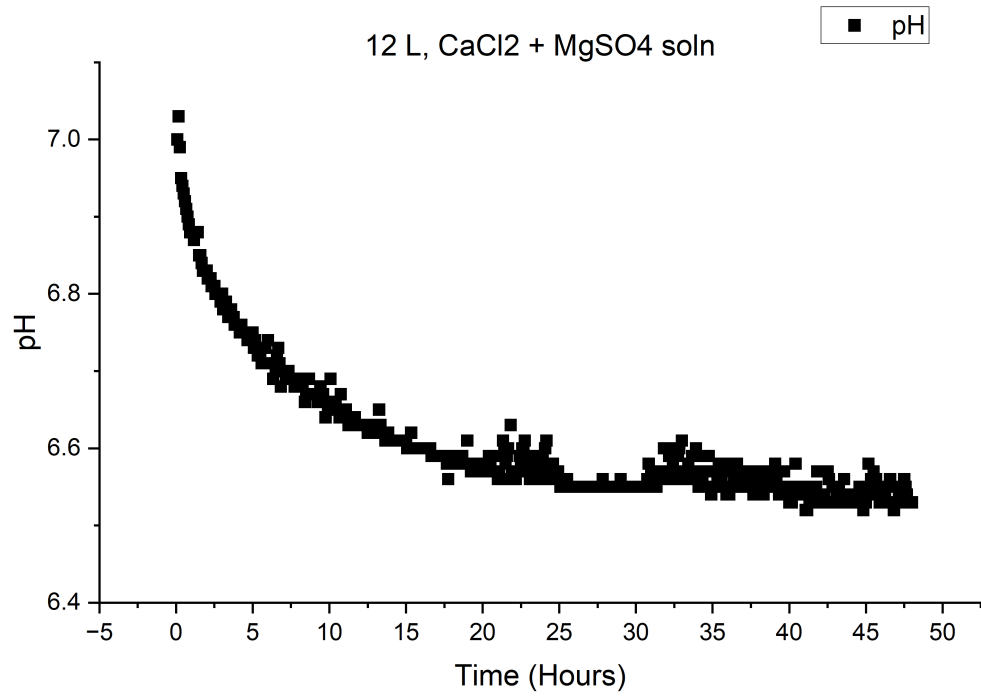


**Figure B3:** pH over time for 12 L of solution 5A left open to atmosphere.

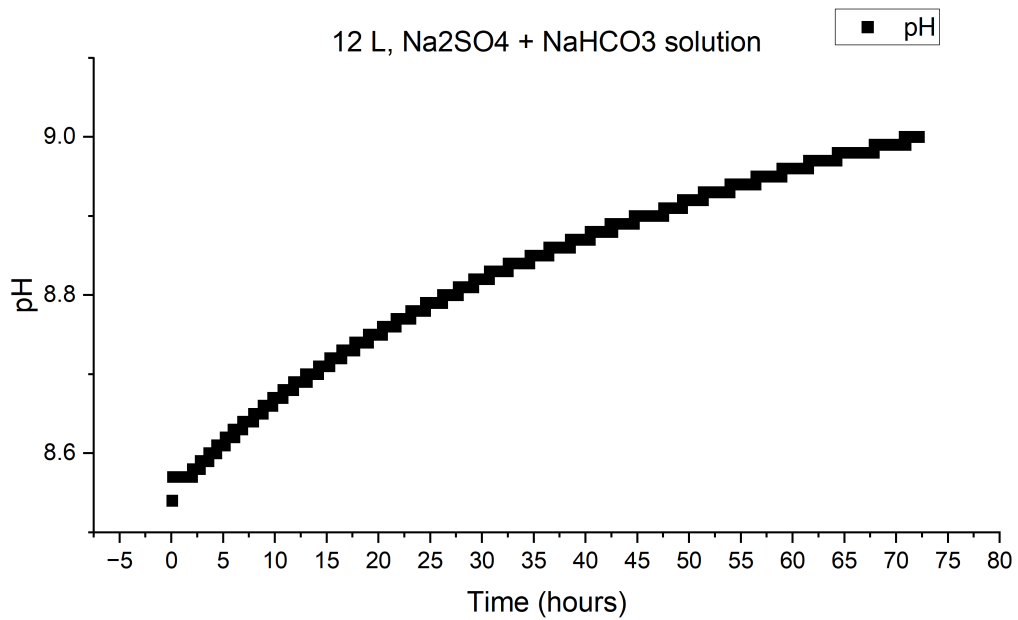


**Figure B4:** pH over time for 12 L of solution 5B left open to atmosphere.

The results of these experiments show that although the solution 5A at 6 L reaches equilibrium roughly around 16 hours when the solutions had been being used, solution 5B was still releasing CO<sub>2</sub> after 48 hours. These results show that the main reason for the difference in turbidity between different volume batches of solution is that solution 5B is not at equilibrium at 16-24 hours. This means that due to previously mentioned factors, the 6 L batch had a lower carbonate concentration and higher pH than the 12 L batch. Of these two factors, the lower carbonate concentration reduces calcite precipitation, while the increased pH lowers the solubility of calcite and increases precipitation, since calcite precipitates based on equation B3, and the concentration of CO<sub>3</sub><sup>2-</sup> increases with pH, as shown in equation B2.

Based on the results showed in tables B1 and B2, the pH factor is more important, and therefore the difference in pH between 6 L batches and larger batches is the driving factor in the difference in turbidity. The incorrect assumption that both solutions were at equilibrium after 16 hours not only made it impossible to scale the solution preparation without drastically changing the degree of supersaturation in the solution, but it also introduced variability in all experiments even at 6 L as the exact time between solution preparation and running the experiment (i.e. whether the solution was open for 16 hours or 24 hours) changed the degree of supersaturation, and therefore the resulting turbidity. Furthermore, the exact times between solution preparation and an experiment were not noted, so these changes are impossible to account for.

To solve this problem, two methods were available. The first was to allow solutions to fully reach atmospheric equilibrium, verified by pH and conductivity readings. As shown in figure B4, especially when moving into higher volumes of solution, the amount of time needed to reach equilibrium in a quiescent solution is untenable. To speed up this process, a mechanical

intervention would be needed, either a fan apparatus to increase the airflow across the surface of the solution, or a stirring apparatus to increase the dispersion of carbonate inside the solution, or a combination of both. Additionally, both these solutions would significantly increase the rate of evaporation and that would also need to be factored in and corrected for. The second method is to minimize the interaction with atmospheric gasses. This can be achieved by immediately capping the solutions after the components are combined and using them as soon as they are fully mixed. This method has the advantage of simplicity, both in not having to construct a new apparatus and not requiring detailed planning on timing to use a solution. Though this method requires new solutions to be prepared for each individual experiment on days where multiple will be run, it is still the best option.

Unfortunately, to use solutions that did not interact with the atmosphere, new solutions needed to be developed. The solutions that have previously been used, when not allowed any gas exchange, produce too low of turbidities to be useful in determining the relative effectiveness of different parameters. An experiment run with the same parameters as table 1, with the only difference being the experiment was run immediately after the solutions were prepared instead of the following day, resulting in a turbidity of less than 2.

To devise these new solutions, several factors were considered. The solution should match as closely as possible the composition of brine solutions produced in actual desalination plants. The solution should have a wide gap between the turbidities produced in less effective sets of parameters (for this measurement, rotelle is used as a negative control as it is significantly worse performing than the other three shapes) and more effective sets of parameters. The solution should produce turbidities that are high enough so that variation and noise in the turbidity measurements do not obscure the larger trends. Finally, the turbidities produced need to be low

enough the turbidity measurements are accurate, and that there is no significant deposition (where the calcite crystals form and fall out of solution, not leaving the static mixer, causing turbidity measurements to no longer be a good approximation for crystal formation, as well as potentially impacting the fluid dynamics of the static mixer).

Sampling data of the composition of brine solutions in Southern California inland desalination plants, shown in figure B5, is selected as a target<sup>3</sup>.

parameters	DWTP no. 1	DWTP no. 2	DWTP no. 3	section A	section B		section C	
	site S1	site S6	site S3	site S2	site S4	site S5	site S7	site S8
pH	7.8	7.7	7.7	7.9	7.8	7.7	7.9	7.9
alkalinity (mg/L as CaCO <sub>3</sub> )	1629 ± 8	1588 ± 25	508 ± 16	1638 ± 14	663 ± 0	658 ± 36	1017 ± 16	1013 ± 0
Ca <sup>2+</sup> (mg/L)	840 ± 10	1178 ± 29	847 ± 45	827 ± 35	870 ± 37	905 ± 13	968 ± 19	943 ± 83
Mg <sup>2+</sup> (mg/L)	301 ± 6	293 ± 3	154 ± 7	302 ± 13	149 ± 47	187 ± 4	218 ± 4	210 ± 16
Na <sup>+</sup> (mg/L)	464 ± 18	674 ± 20	977 ± 34	510 ± 24	912 ± 4	742 ± 23	818 ± 6	699 ± 48
NO <sub>3</sub> <sup>-</sup> (mg N/L)	65.2	104.8	31.4	68.1	39.8	87.8	62.4	107.6
NO <sub>2</sub> <sup>-</sup> (mg N/L)	ND <sup>a</sup>	ND <sup>a</sup>	1.3	ND <sup>a</sup>	1.2	0.2	0.6	0.3
NH <sub>4</sub> <sup>+</sup> (mg N/L)	ND <sup>a</sup>	ND <sup>a</sup>	1.0	ND <sup>a</sup>	0.7	0.1	0.4	0.1
PO <sub>4</sub> <sup>3-</sup> (mg P/L)	0.1	0.3	5.9	0.1	7.6	3.6	4.5	2.5
SO <sub>4</sub> <sup>2-</sup> (mg/L)	1101 ± 24	1490 ± 53	1031 ± 89	1104 ± 6	995 ± 18	558 ± 12	1149 ± 47	932 ± 24
Cl <sup>-</sup> (mg/L)	897 ± 7	1531 ± 11	2574 ± 36	909 ± 25	2340 ± 21	2371 ± 4	2013 ± 47	2046 ± 4
H <sub>4</sub> SiO <sub>4</sub> (mg Si/L)	51 ± 2	52 ± 0	56 ± 1	52 ± 1	62 ± 0	62 ± 1	49 ± 1	41 ± 6
FSS(mg/L)	0.8	1.9	40.4	0.4	31.6	10.9	17.7	6.5
TSS (mg/L)	1.5	4	52.4	0.9	42.9	18.3	24.1	11.9
TDS (mg/L)	3268	4608	5258	3364	5153	4709	4844	4733
DOC (mg C/L)	5.9	5.0	3.1	6.5	3.1	3.5	3.9	3.8

<sup>a</sup>Nondetectable.

**Figure B5:** Water composition data taken from brine solutions collected at various inland sites in Southern California.

Using site 1 as a model, the amount of the four salts used for solution preparation, Na<sub>2</sub>SO<sub>4</sub>, CaCl<sub>2</sub>, NaHCO<sub>3</sub>, and MgSO<sub>4</sub>, are calculated to match the calcium, magnesium, sodium, sulfate, chlorine and carbonate ion concentrations. Table B3 shows the resulting masses of salts to be combined per 1 L of water to approximate brine from site 1, while table B4 shows the resulting ion concentrations calculated using OLI Stream Analyzer® compared to the concentrations from site 1.

**Table B3:** Components of proposed new solution.

Component	Total amount (g)	CaCl <sub>2</sub> + Na <sub>2</sub> SO <sub>4</sub> Solution, amounts added (g)	MgSO <sub>4</sub> + NaHCO <sub>3</sub> Solution amount added (g)
H <sub>2</sub> O	1000	500	500
CaCl <sub>2</sub> (dh)	3.087	3.087	0
MgSO <sub>4</sub> (heptahydrate)	3.053	0	3.053
Na <sub>2</sub> SO <sub>4</sub>	0.276	0.276	0
NaHCO <sub>3</sub>	1.368	0	1.368

**Table B4:** Resulting concentrations of select ions in new solution, calculated from OLI simulation and literature values for brine from site 1<sup>3</sup>.

Species	DWTP no. 1, (mg/L)	Proposed new solution, combined, (mg/L)
Alkalinity as CaCO <sub>3</sub>	1629 +/- 8	1633
Ca <sup>2+</sup>	840 +/- 10	842
Mg <sup>2+</sup>	301 +/- 6	301
Na <sup>+</sup>	464 +/- 18	464
SO <sub>4</sub> <sup>2-</sup>	1101 +/- 24	1227
Cl <sup>-</sup>	897 +/- 7	1489

In order to perfectly match the concentration of the two most important species for calcite precipitation, carbonate and calcium ions, using only those four salts, the concentrations of sulfate and chloride ions were outside the literature range. This was deemed acceptable because although excess ions will slightly affect the activity of the solution neither directly affects calcite precipitation.

The final, very important, component of the new solution was the pH. Though more information on the specific sampling method would help better recreate the brine solution from literature, the paper stated that sample bottles were collected and the samples were analyzed, “within 2 hours” for pH<sup>3</sup>. In the time between generation of the brine and the time that the sample was analyzed, some calcite was theoretically crystallizing. As calcite crystallizes, according to equation B3,  $\text{CO}_3^{2-}$  is removed from the solution, causing  $\text{H}_2\text{CO}_3$  and  $\text{HCO}_3^-$  ions to lose their hydrogen ions according to equation B2, lowering the pH of the solution. Since even if the pH was taken as close to the generation of the brine as possible (and based on the language in the paper, it doesn't seem that minimizing time was a main priority), it is safe to say that the brine at the instantaneous moment of generation had a pH of higher than 7.8. However, due to the uncertainty of the kinetics of calcite precipitation in these exact brine solutions and the un-specificity of the exact sampling procedure used, calculating an exact value is impossible. Furthermore, any interaction with atmospheric gases, as has been shown with solution 5, will result in the release of  $\text{CO}_2$  gas and the further raising of the brine solution's pH.

Based on OLI calculations, the two proposed solutions have a pH of 7.03 and 7.91. While again there is no real way to calculate an instantaneous pH without crystallization after the two solutions are mixed, it can be said that this theoretical pH is lower than the lowest possible target

pH. To fix this issue, adding a small amount of NaOH to one or both of the solutions to raise the pH of the resulting mixed solution is explored.

To begin, OLI are ran looking at the pH of the mixed solution after it reached equilibrium with a variable amount of NaOH added. On one end of the spectrum, with no NaOH added the solution, at equilibrium the pH is 6.37 (again, the precipitation of calcite drives the pH of the combined solution significantly lower than the pH of either individual component). On the other end, to achieve an equilibrium pH of 7.8, 0.62 g/L NaOH is needed. Therefore, depending on the exact sampling procedure used, to match the literature brine composition exactly, some NaOH is needed, but less than 0.62 g/L, and it is impossible to calculate an exact amount, though it is likely much closer to 0 g/L than 0.62 g/L.

Given the range of NaOH additions that could be plausibly argued, the best course of action is to pick a value that satisfied the goals of a new solution, namely a resulting turbidity after being run through the static mixer that is in a useful range, and a significant gap in turbidity between the best and worst sets of parameters. As a starting point, a benchtop experiment was conducted that involved taking two 20 mL aliquots of the component solutions, adding them to a beaker with a stir bar set to a constant setting for an amount of time, and then taking a turbidity measurement.

To begin, solution 5 was selected as a point of reference, since solution 5 after 24 hours of exposure to atmosphere at 6 L is known to fit the above criteria. After working out the issues in experimental design and determining that the order in which the solutions are added to the beaker had a significant impact, an experiment was run on solution 5 open to the atmosphere over time. The results are shown in table B5.

**Table B5:** Results of benchtop experiment combining aliquots of solution 5A with 5B, then measuring turbidity after time.

Time exposed to atmosphere (hour)	Time stirred before sampling (min)	Order added to beaker	Turbidity measurements (NTU)	Average turbidity (NTU)
1	2	A-B	153, 99.3, 94.7	116
1	2	B-A	55.2, 38.5, 75.4	56.3
3	2	A-B	88.2, 135, 123	115
3	2	B-A	36.3, 18.8, 80.3	45.1
23	1	A-B	43.7, 36.9	40.3
23	1	B-A	54.4, 44.0	49.2
23	2	A-B	152, 143, 131	142
23	2	B-A	173, 159, 153	162
23	3	A-B	216, 219	218
23	3	B-A	235, 248	242

The main takeaways from this experiment are a confirmation of what has been previously shown, that the longer the two component solutions are allowed to interact with the atmosphere, the higher the turbidity, and an approximate target range of turbidities for the new solution.

The same experiment is then conducted using solutions with the salt concentrations shown in table B3, with a variable amount of NaOH added to these solutions. Three different NaOH amounts were tested, with the results shown in table B6.

**Table B6:** Results of benchtop experiment combining aliquots of the solutions shown in table B3 with variable amounts of NaOH added, then measuring turbidity after time.

Mass of NaOH added, per 1 L of resulting mixed solution (g)	Time stirred before sampling (min)	Order added to beaker	Turbidity measurements (NTU)	Average turbidity (NTU)
0.10	2	12A – 12B	158, 152, 183	164
0.10	2	12B – 12A	76.1, 85.1, 57.9	73
0.30	2	12A – 12B	370, 421, 387	393
0.30	2	12B – 12A	248, 255, 237	247
0.1375	1	12A – 12B	150, 142	146
0.1375	1	12B – 12A	80.0, 91.2	85.6
0.1375	2	12A – 12B	208, 173, 175	185
0.1375	2	12B – 12A	102, 96.9	99
0.1375	3	12A – 12B	183, 219	201
0.1375	3	12B – 12A	131, 94.0	113

The takeaways from this set of experiments are that 0.1375 g NaOH per 1 L mixed solution is a reasonable starting point to take to the static mixer, and that this solution has significantly different crystallization kinetics compared to solution 5. The resulting turbidities at three different stirring times of solution 5 after 23 hours and the new solution with 0.1375 g/L NaOH added are plotted figure B6.

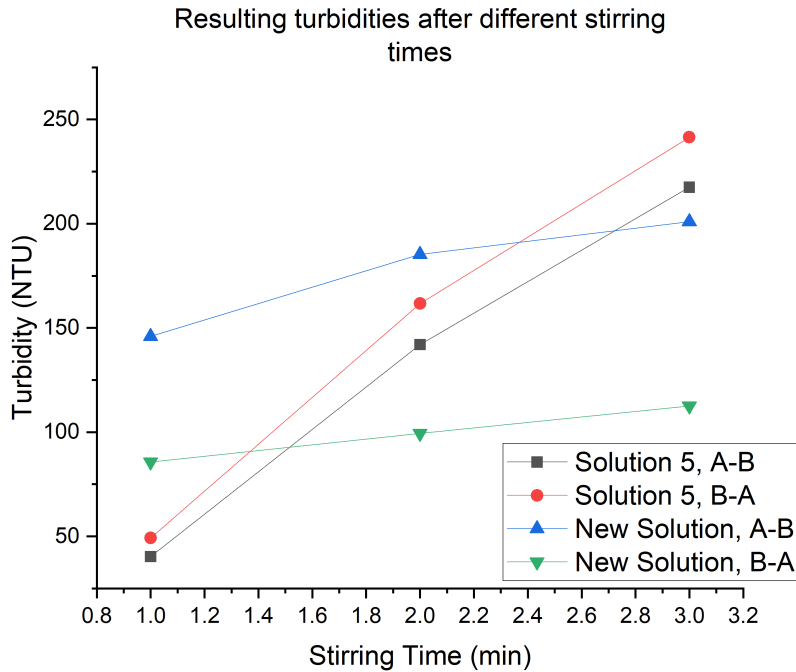


**Figure B6:** Measured turbidities after different times for aliquots of solution 5 and the new solution shown in B3 and 0.1375 g/L NaOH.

It is unclear what the effect of these different kinetics on static mixer experiments will be, but for now it is worth noting that the crystallization of solution 5 is much more dependent on time since mixing than the new solution.

Next, the new solution with 0.1750 g/L NaOH is used for a static mixer experiment. Using PETG shells, 1" diameter, 48" length and a residence time of 11 minutes, the resulting turbidity was 169, much higher than necessary. Next, an experiment is conducted with the same set of parameters, only with 0.075 g/L NaOH added instead. This resulted in a turbidity of 66.1 NTU, well within the useful range. The final criterion for an effective new solution is a large gap between an effective run and an ineffective run. To test this, an experiment was conducted with this same solution, diameter, length, residence time and material, except with rotelle instead of

shell as the mixer shape. Rotelle was selected because it was shown to perform worse than the other three shapes consistently across residence times and materials. This experiment resulted in a turbidity of 11.2 NTU at 90 minutes, showing this solution provides that necessary gap. Subsequent experiments used the salt concentrations shown in table B3 with 0.075 g/L NaOH added, referred to as “solution 6”.

**C: Additional Kolmogorov mixing length plots**

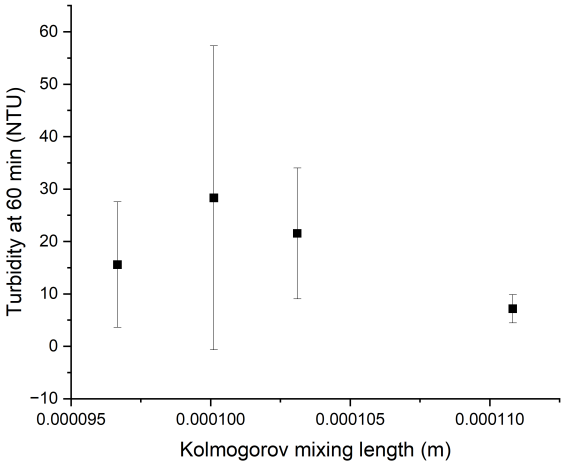


**Figure C1:** Average turbidities at 60 min for each shape with data using a 3 min residence time, at 0.5” diameter, PETG, 48” length and solution 5 plotted against Kolmogorov mixing length.

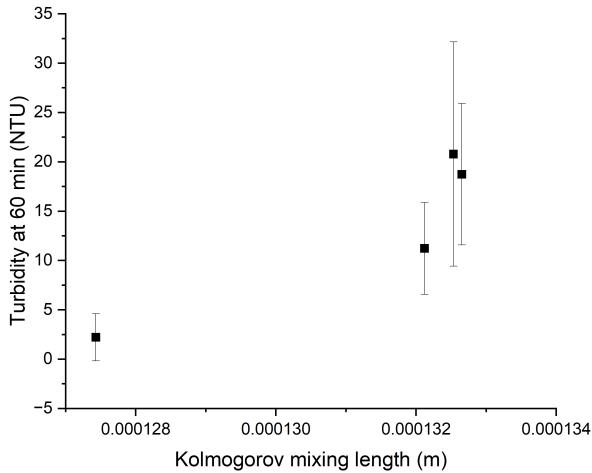


**Figure C2:** Average turbidities at 60 min for each shape with data using a 7 min residence time, at 0.5” diameter, PETG, 48” length and solution 5 plotted against Kolmogorov mixing length.

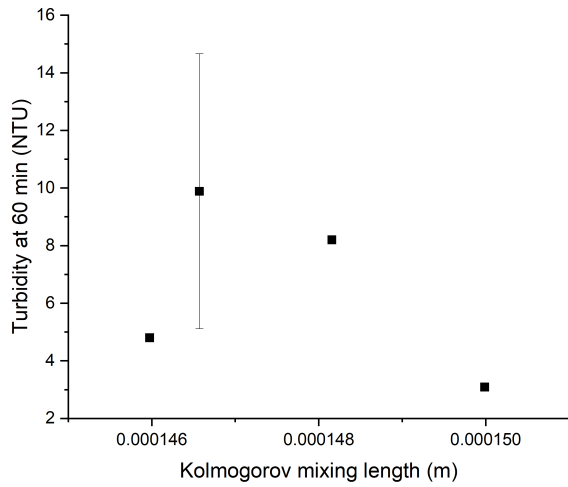


**Figure C3:** Average turbidities at 60 min for each shape with data using a 11 min residence time, at 0.5” diameter, PETG, 48” length and solution 5 plotted against Kolmogorov mixing length.

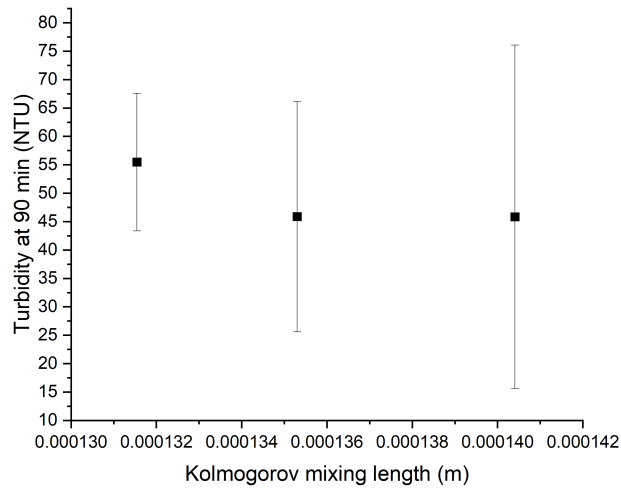


**Figure C4:** Average turbidities at 60 min for each shape with data using a 11 min residence time, at 0.5” diameter, PETG, 48” length and solution 5 plotted against Kolmogorov mixing length.

## D: Residence time distributions

**Table D1:** Variance and skewness for a step input residence time distribution at a 7 min nominal residence time, 1” diameter and 48” length tubing, using conductivity to measure the concentration of a NaCl solution.

	Variance	Skewness
Shell	151.50	303.16
Rotelle	173.63	48.57
Farfalle	698.01	542.51
Hourglass	877.46	816.70

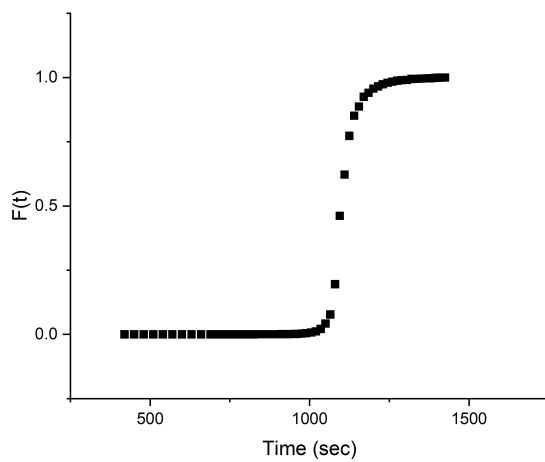


**Figure D1:**  $F(t)$  plot for the RTD of shell at a 7 min nominal residence time, 1” diameter and 48” length tubing.

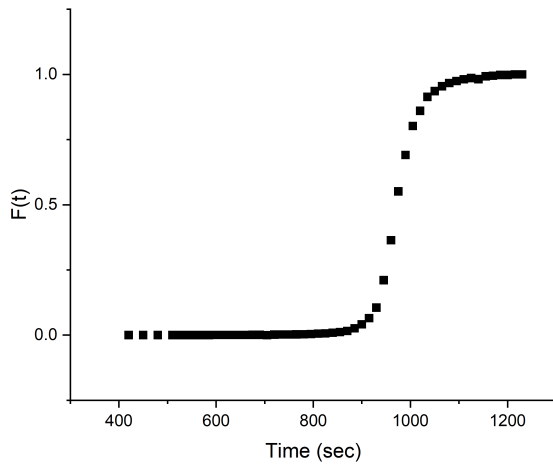


**Figure D2:**  $F(t)$  plot for the RTD of rotelle at a 7 min nominal residence time, 1" diameter and 48" length tubing.

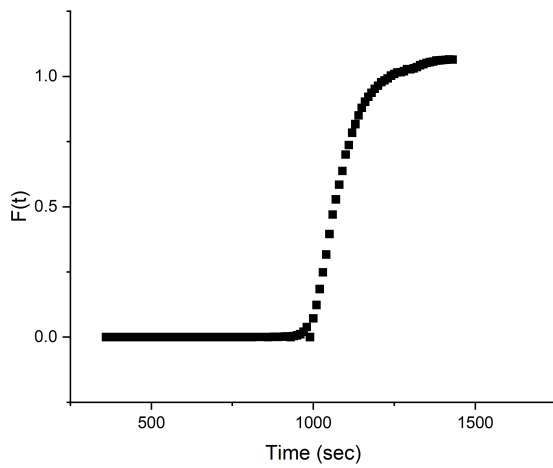


**Figure D3:**  $F(t)$  plot for the RTD of farfalle at a 7 min nominal residence time, 1" diameter and 48" length tubing.

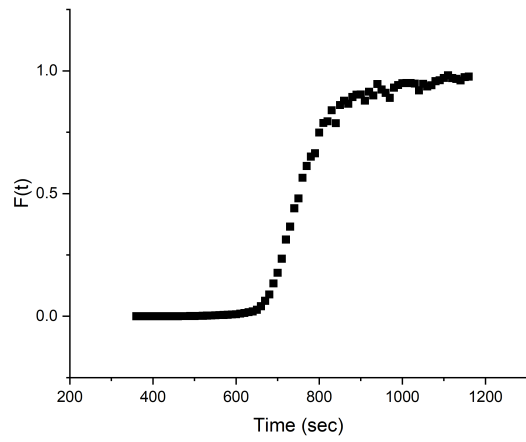


**Figure D4:**  $F(t)$  plot for the RTD of hourglass at a 7 min nominal residence time, 1” diameter and 48” length tubing.